The Timing of Vein Hosted Copper Mineralization and its Structural Setting in The Upper Paleozoic Sedimentary Rocks of Southwest Ireland

Abbreviated title: Cu Mineralization of Southwest Ireland

Jürgen Lang[1,2*], Patrick A. Meere[1], Richard P. Unitt[1] and David Selby[3]

[1] Irish Centre for Research in Applied Geosciences (iCRAG), School of Biological, Earth and Environmental Sciences, University College Cork, Distillery Fields, North Mall, Cork, Ireland

[2] Actual address: GeoZentrum Nordbayern, Friedrich-Alexander-Universität Erlangen-Nürnberg, Schlossgarten 5, D-91054 Erlangen, Germany

[3] Department of Earth Sciences, University of Durham, Durham, DH1 3LE, UK

*Corresponding author: juergen.ohmden@gmail.com

Abstract

This study provides a new insight into the genetic and chronological development of the vein hosted copper sulfide mineralization in the Late Paleozoic Munster Basins of SW Ireland. Field mapping, supported by drone photogrammetry, petrography, microthermometry and geochronology of selected historic mining sites in West Cork reveal elementary data for a reinterpretation of the mineralization processes. Structural investigations define two distinct ore forming episodes: The initial vein precipitation is directly related to syn-basinal, extensional E-W to ENE-WSW striking normal faults. Smaller sediment hosted Cu sulfide occurrences are related to the extensional fault systems. The second mineralization phase occurred during the early stage of the late Carboniferous Variscan compression by reactivation of early extensional, basinal fault systems. Copper mineralization related molybdenite samples from the historical Ballycummisk Mines on Mizen Peninsula produced

Re-Os dates of 315.5 ± 1.6 Ma and 311.8 ± 1.6 Ma. This Pennsylvanian (Upper) Carboniferous sulfide emplacement is related to this second stage, syn-Variscan compressional mineralization event. The discovery of the two distinct Cu mineralizing events in SW Ireland provides an important contribution to the understanding of the development of the Irish Ore Field including the Pb-Zn Midlands Deposits.

Keywords: copper mineralization, SW Ireland, Variscan, Munster Basin, Re-Os geochronology, fluid inclusions

Supplemental material:

Local Observations (detailed description of local observations shown in Figure 3 and Table 2.

Methodology Details (extended version of the Methodology with detailed descriptions).

Appendices:

Appendix Table A1: Locations of selected samples from West Cork, SW Ireland

Appendix Table A2: Fluid inclusions measurements of selected locations and historic copper mines from Southwest Ireland.

Introduction

The copper occurrences of SW Ireland have been utilized for over 3500 years (Williams 1991). Bronze Age (O’Brien 1987) sites on the Mizen Peninsula (Figs 1 and 2) show that the original extraction of Cu ore targeted surficial malachite stained, sediment-hosted mineralization. The heyday of Cu mining in SW Ireland was between 1812 and 1885 when an estimated total of 284,500 tonnes of vein-hosted ore was extracted from Mountain Mine at Allihies, the most productive mine in the area (Fig. 2; O’Brien 1959; Williams 1991). Many smaller mines were also active throughout West Cork during the 19th century (Reilly 1986).

The timing of Cu deposits in SW Ireland has previously been described as syn- to post-Variscan (Sheridan 1964; Halliday and Mitchell 1983; Wen *et al.* 1996; Meere and Banks 1997; Spinks *et al.* 2016) although a recent study (Lang *et al.* 2020) has demonstrated that major mineralization, associated with E-W trending basin forming structures are pre-Variscan in age.

Wen *et al.* (1996) and Snodin (1972) identified sediment hosted mineralization in stratigraphically bound, reduced green sandstone zones (green beds; Fig. 2b). The sediment-hosted stratiform copper (SSC) occurrences are associated with channel sandstones near the base of the Toe Head Formation and within the upper part of the Castlehaven Formation (Reilly 1986; Fig. 2). Spinks *et al.* (2016) measured negative $\delta^{34}S$ values at Allihies caused by biogenically induced reduction within the Old Red Sandstone Facies resulting in syngenetic-diagenetic sulfide mineralization.

The vein hosted deposits at Crookhaven (Fig. 2) have been described as saddle reef tension gashes exposed in an anticlinal (Variscan) core (Duffy 1932 and Reilly 1986). Reilly (1986) considered a late syntectonic age for this mineralization. Halliday and Mitchell (1983) dated clay minerals from Allihies (Fig. 2), which were sampled from the wall rock next to the quartz veins. The K-Ar dates showed results between 290 and 261 Ma for the Mountain Mine Lode. An older age of 321 Ma was measured for an apparently unmineralized quartz vein (Halliday and Mitchell 1983). Sanderson (1984) described N-S trending mineralized veins on Beara Peninsula with strong folding and cleavage, which led to a proposed pre/syn-Variscan age. Faulting and brecciation of mineralized veins on Mizen Peninsula (Fig. 2) has been confirmed by Reilly (1986). For Crookhaven, Reilly (1986) considered a late syn-tectonic age for mineralization.

According to Wen *et al.* (1996) and Spinks *et al.* (2016) the early sediment-hosted sulfides were remobilized by metamorphic fluids into late- or post-Variscan quartz veins. This remobilization was driven by non-magmatic, metamorphic (Variscan) fluids which were capable of dissolving and reprecipitating the sulfides (Wen *et al.* 1996; Spinks *et al.* 2016). Wen *et al.* (1996), Meere and Banks (1997), as well as Spinks *et al.* (2016) interpreted post-Variscan N-S extension as the major driver behind the sulfide remobilization and mineralization event with large quartz vein precipitation along normal faults.

Recent findings (Lang *et al.* 2020) show cleaved and folded N-S and E-W striking mineralized quartz veins at Allihies. Some of the pre-Variscan copper lodes where sinistrally off-set by Variscan compressional faults. Vein mineralization related molybdenite yielded Re-Os dates from the Allihies Copper mines of 367.3 ± 5.5 to 366.4 ± 1.9 Ma (Lang *et al.* 2020). This is interpreted as mineralization related to basin formation and associated N-S crustal extension (Lang *et al.* 2020).

Previous fluid inclusion microthermometry measurements of quartz veins from Mizen Peninsula suggest peak-metamorphic conditions of between 300-400 °C (Wen *et al.* 1996). Homogenization temperatures (T_h) can be as low as 100 °C (Crookhaven; Wen *et al.* 1996). Meere and Banks (1997) indicated medium to moderate salinities (4-16 wt% $NaCl_{equiv}$) for syn-Variscan quartz veins and high salinities (22-27 wt% $NaCl_{equiv}$) for "apparently" post-orogenic extensional veins at Allihies. Recent detailed measurements from Allihies copper mines range from moderate salinity and higher homogenization temperatures (T_h LV-L = <314 °C; >3.2 %$NaCl_{equiv.}$) to high salinities and very low homogenization temperatures (T_h LV-L = >74 °C; <28.5 %$NaCl_{equiv.}$) for the mineralized pre-Variscan quartz veins (Lang *et al.* 2020). Syn-Variscan quartz veins (en echelon tension gashes) show low to moderate salinities and T_h values of about 200 °C.

This paper focusses on selected localities and historic mines from the Upper Paleozoic Munster and South Munster Basins (Figs 1 and 2) to develop a regional model for vein hosted Cu mineralization.

Geological Setting

Tectonostatigraphic framework of the Upper Devonian Munster Basin

North-south crustal extension between the Middle and Upper Devonian, saw the development of a large half-graben basin in southern Ireland, the Munster Basin (Naylor and Jones 1967). The east-west trending Coomnacronia-Killarney-Mallow Fault Zone (CKMFZ) marks one of the main northern bounding structures of this intracratonic basin (Fig. 1; Ennis *et al.* 2015 and references therin).

The basin infill is dominated by late Middle to Upper Devonian northerly derived alluvial/ fluvial generally fine-grained siliciclastic sediments (Fig. 2; MacCarthy 1990). Detailed stratigraphic nomenclature is described by Williams *et al.* (1989), MacCarthy (1990), Williams (2000), MacCarthy *et al.* (2002) and Pracht and Sleeman (2002, Fig. 2a and 2b):

Continued subsidence and development of the South Munster Basin was triggered by normal movement on the east-west trending Cork-Kenmare Fault Zone (CKFZ) at the end of the Devonian (Fig. 1; MacCarthy 2007). The concomitant marine transgression from the south resulted in the accumulation of marine siliciclastics within the South Munster Basin south of the CKFZ and limestones on a more stable platform to the north (Fig. 2; MacCarthy 2007).

NNW-directed compression (Fig. 1) terminated sedimentation towards the end of the Carboniferous and marked the beginning of the Variscan Orogeny (Sanderson 1984; Ford 1987; Meere 1995b; Quinn *et al.* 2005). According to Ar/Ar dates of cleaved and deformed intrusive rocks on Beara Peninsula (Fig. 2a; Pracht and Timmerman 2004; Quinn *et al.* 2005), the initial effect of the Variscan compression started before 318 Ma/314 Ma. The orogeny resulted in crustal shortening of over 52% with the development of a pervasive cleavage, followed by kilometre scale buckling and faulting (Fig. 2a; Cooper and Trayner 1986; Ford 1987). The folding and faulting followed a general NE-SW structural strike in the west (Fig. 2a; GSI 2016). High-angle basin-controlling faults were reactivated during compression (Price and Todd 1988). Reverse NE-SW-trending faults, as well as rarer NW-SE-trending strike slip faults are described by Meere (1995c) occurring in the west of the Munster

Basin. The sediments underwent metamorphism to sub-greenschist facies (Meere 1995b).

Minor intrusions previously described as alkali basalts, trachytes and phonolites occur around Beara Peninsula and the northern Sheep's Head coastline (Boldy 1955; Viswanathiah 1959 and Reilly 1986; Pracht and Kinnaird 1997; Pracht 2000; Figs 1 and 2). Pipe-like lamprophyric intrusions dated at 318 ± 3Ma (Ar/Ar kaersutite; Pracht and Timmerman 2004) and 314.44 ± 1.00 Ma (Ar/Ar phlogopite; Quinn *et al.* 2005) have been studied at Black Ball Head (5.6 km south of Allihies, Fig. 2) and were formed during the early Variscan compression (Pracht and Kinnaird 1995; Pracht 2000). Post Variscan undeformed trachytic dykes from White Ball Head (400 m northwest of Black Ball Head) show ages of 296.88 ± 0.60 Ma (Ar/Ar phlogopite) (Quinn *et al.* 2005).

Methodology

For more details about the Methodology please see Supplemental material: Methodology Details.

The examined study areas (Fig. 3) were selected based on their historical mining importance, and their ability to demonstrate a clear structural history. Field mapping in the selected areas focussed primarily on the classification and sampling of mineralized and unmineralized quartz veins, as well as mineralized sedimentary units (App. Table A1). Structural measurements and veining cross-cutting relationships were utilised for relative chronology. Aerial drone mapping was used to contextualise features identified in the field.

Large scale structures identified in the field were traced on open access satellite maps to identify the overall structural pattern (Fig. 3; Bing™ Satellite Maps 2016-2019; Google Maps 2016-2019; ArcGIS BaseMaps 2016-2020). Offshore bathymetry data (Geological Survey Ireland, Infomar 2017) provided additional bedrock information around Mizen Peninsula (Fig. 3).

Quartz vein samples and ore samples were collected from all selected study areas. In-situ samples were taken whenever possible. In some cases, where the historic mine shafts were not accessible or due to the lack of outcrop (Ballycummisk, Fig. 3), it was necessary to collect samples from spoil material.

The samples were petrographically analysed as polished blocks and polished thin sections using transmitted and reflected light microscopy. Images were captured using a Leica (DVM2500) digital microscope with an attached VZ700C lens in the Geomicroscopy Facility at University College Cork (UCC).

Pre-Variscan and syn-Variscan quartz veins were classified in the field according to their structural genesis such as extensional or compressional tension gashes. Five mineralized and seven unmineralized (barren) quartz vein samples were prepared as doubly polished thin sections. Small chips of max. 0.5 cm^2 were examined with a Linkam (LMS600) temperature-controlled microscope stage, combined with an Olympus BX50 microscope, a x100 LWD objective and an attached 16 megapixels Nikon DS-Ri2 camera at the UCC Geomicroscopy Facility. Bi-phase (liquid and vapour, L+V) fluid inclusions were analysed for their freezing temperature T_{ice}, the first melt temperature T_{fm} and the final melt temperatures T_m, as well as the homogenization temperature T_h = liquid + vapour = liquid. Within the mineralized veins, primary inclusions were selected, which are genetically related to the copper sulfides (App. Table A2). Salinity was calculated as wt% $NaCl_{equiv}$ by using the Excel macro HOKIEFLINCS_H2O-NACL (Steele-MacInnis *et al.* 2011; Steele-MacInnis *et al.* 2012; Bodnar 1993; Atkinson 2002; Bodnar *et al.* 1994; Bodnar 1983).

A historic molybdenite sample (BM.1964,R230) collected by Sir Arthur Russell in 1907 from the Ballycummisk Mine dumps was obtained from the National History Museum in London (NHM) (Fig. 3). This study also discovered an additional molybdenite sample from the Ballycummisk Mine dumps (Table 3, JL_BC_525). Both samples contain fine-grained molybdenite with crystal size smaller than 2 mm. They were both analysed using reflected light microscopy and fluid inclusion microthermometry for JL_BC_525. Both samples underwent Re-Os molybdenite geochronology at Durham University Durham Geochemistry Center. Sample preparation and analysis utilised established analytical protocols (Selby and Creaser, 2001; Li *et al.*, 2017). Approximately 20 mg of pure molybdenite with aqua regia (3 ml HCl + 6 ml HNO_3) and a known amount of tracer solution (^{185}Re + isotopically normal Os) was digested and equilibrated in a carius tube in an oven for 24 hrs at 220˚C. The Os and Re were purified from the acid solution using solvent extraction, microdistillation and anion chromatography. The purified Re and Os fractions were measured for their isotopic compositions in static mode using a Thermo Scientific Triton mass spectrometer. The Re-Os data and calculated dates are presented in Table 3. Model dates are presented including all analytical sources of uncertainty and the decay constant uncertainty.

Results

Large areas of outcropping bedrock, especially on the West Cork peninsulas and south-western coastline greatly facilitates the structural interpretation of satellite imaging data and kilometre scale geological features (large-scale, peninsulas, see table 1). The detailed aerial image interpretation is ground truthed for selected localities (Fig. 3).

In this study two major structural events were identified: A syn-basinal, pre-Variscan extension, causing E-W to ENE-WSW striking normal faults; and a syn-Variscan compressional event causing cleavage formation, folding and reverse faulting with a general NE-SW strike. Selected localities are used as case studies to show the relationship of the Cu mineralization to these structural events (Fig. 3). Syn-extensional, pre-Variscan geological features show partial syn-compressional, syn-Variscan overprints. The most important local observations are shown in table 2 (including Figs 4-9). For detailed description of all localities see Supplemental material: Local Observations. The selected sample locations are available in Appendix Table A1.

In the northernmost part of the research area, the Beara Peninsula (Fig. 1, 2a and 3), East-West striking faults and fault systems are identified as negative topographic features (photolineaments) on satellite imaging data (Bing™

Satellite Maps 2016-2019). Owing to surficial weathering the faults form trenches of about 3 to 40 metres width and up to 8.4 kilometres length (Fig. 3). These faults have a mean strike direction of 089° (N = 301). Along the coastline the faults often form narrow elongate bays due to preferential marine erosion. Sometimes, the faults are associated with large (up to several hundred metres) E-W trending quartz veins. Many of these form historically mined copper lodes (Geological Survey Ireland Jetstream 2019; Fig. 3, e.g. Allihies and north coast of Beara Peninsula). Perpendicular N-S striking faults up to 4.3 km in length are generally not associated with quartz veins, apart from Allihies (Fig 3). Owing to their nearly parallel orientation to the Variscan compression the N-S faults show stronger folding than the E-W faults (nearly perpendicular to Variscan stress).

On Sheep's Head Peninsula (Fig. 1, 2a and 3) the E-W faults have a maximum length of 4.7 km and a mean strike of 089 (N = 63). Like the Beara Peninsula the E-W faults are associated with historically mined, mineralized quartz veins (Fig. 3, e.g. Gortavallig and Killeen North). N-S to NNE-SSW striking faults with a maximum length of up to 5 kilometres are also present.

The southern part of Mizen Peninsula (Fig. 1, 2a and 3) is dominated by ENE-WSW striking faults, which belong to the same fault system as the E-W faults on Beara Peninsula and Sheep's Head. These ENE-WSW faults can be followed offshore (Geological Survey Ireland Infomar 2017). Their mean strike is 082° (N = 115) and the faults can have a maximum length of 7 km (Fig. 3). The north-eastern part of Mizen Peninsula shows more an E-W strike of these faults with max. 4.3 km length and a mean strike of 090° (N = 98). The E-W striking, as well as the ENE-WSW striking faults can sometimes be associated with the historic copper lodes (Fig. 3, e.g. Dhurode Mine and Crookhaven Mines). N-S striking faults on Mizen Peninsula have a maximum length of 6.6 km and are generally not associated to mineralized quartz veins.

Molybdenite Re-Os geochronology

The fine grained (grain size < 2 mm) historic molybdenite sample from the Ballycummisk tailings (BM.1964,R230; Fig. 3; App. Table A1) possesses 70.7

± 0.3 ppm Re, 44.4 ± 0.2 ppm ^{187}Re and 231.3 ± 0.7 ppb ^{187}Os (Table 3). The Re-Os data yields to a model date of 311.8 ± 1.6 Ma for molybdenite mineralization. The recent molybdenite finding from the Ballycummisk tailings (Fig. 9c) has a grain size of < 100 µm. It contains 113.5 ± 0.4 ppm Re, 71.3 ± 0.3 ppm ^{187}Re and 375.9 ± 1.2 ppb ^{187}Os. The ^{187}Re-^{187}Os model date is 315.5 ± 1.6 Ma (Table 3).

Fluid inclusion microthermometry of the selected localities

According to their structural formation, 7 quartz vein samples were classified as pre-Variscan veins (mainly E-W to SW-NE striking, 5 mineralized and 2 unmineralized/barren, App. 2). Five unmineralized/barren vein samples were classified as syn-Variscan (en echelon tension gashes, App. 2). The fluid inclusions of both pre-Variscan and syn-Variscan vein types consist of a 2-phase system with a major liquid (L) and a minor vapour (V) phase (Fig. 10a-d, App. 2). No CO_2 phase was detected. Anhedral to subhedral quartz grains prevented a clear identification of individual growth zones. The measured quartz veins show a large amount of secondary and pseudosecondary fluid inclusion trails along healed fractures. These fractures were avoided. The primary fluid inclusions (target for this study) occur as clusters or separate inclusions along growth zones (Goldstein and Reynolds 1994). Primary fluid inclusion assemblages (FIA) were classified individually for each sample (App. 2). The classification criteria for the assemblages are the most finely discriminated, petrographically associated group of coeval inclusions. This incorporates the fluid inclusion shape, the volume of the vapour phase at room temperature, and the spatial distribution (growth zonations) within the vein sample. The complex growth zonations within the quartz vein samples prevented a temporal placement of the individual fluid inclusion assemblages.

Pre-Variscan E-W veins: All mineralized (pre-Variscan) samples show chalcopyrite as major copper ore. Minor amounts of syngenetic arsenopyrite (Dhurode Mine, JL_DH_522) and syngenetic molybdenite (Ballycummisk, JL_BC_525Re) occur (App. 1). Primary (syn-mineralization) fluid inclusion assemblages in the pre-Variscan, early E-W quartz veins are generally oval to angular shaped (Fig. 10a + 10b). They consist of an undersaturated liquid-rich phase, and a vapour phase with 0.5 to 20 volume percent. The individual fluid inclusion assemblages (FIA) show generally a quite narrow spread in salinities and homogenization temperatures for each individual sample location (App. 2, Fig. 11a). However, between the different sample locations, there is a larger spread in T_h and salinities (Fig. 11a, App. 2). The homogenization temperatures T_h range between 90 and 335 °C. Salinities vary between 5.2 and 22.4 wt.% $NaCl_{equiv}$. The mineralized quartz vein sample from Caha Pass (JL_CP_432E, Fig. 3) represents an exemption with fluid inclusion assemblages clustering between 9.2 and 15.3 wt.% $NaCl_{equiv}$ and a T_h range between 125 to 189 °C, as well as showing a more saline FIA (432E.4) with values between 22.3 and 22.4 wt.% $NaCl_{equiv}$ and T_h between 90 and 123 °C (Fig. 11a, App. 2). The mean homogenization temperature T_h of all fluid inclusion assemblages from the early E-W veins is 211 °C with a mean salinity of 11.2 wt.% $NaCl_{equiv}$ (n = 126).

Syn-Variscan veins: Primary fluid inclusions of the compressional, syn-Variscan quartz veins (en echelon, tension gashes) can be elongated (Fig. 10c), but also irregular angular shaped (Fig. 10d). All assemblages consist of a liquid and a vapour phase with 0.1 to 10 vol.% (App. 2). The homogenization temperature T_h ranges from 104 to 270 °C with salinities between 4.8 and 16.7 wt.% $NaCl_{equiv}$ (Fig. 11b, App. 2). Syn-compressional vein samples with fibrous veins and vugs with large (< 5 cm), euhedral crystals were collected near Durrus (Fig. 2a). The euhedral crystals show assemblages with a T_h from 174 to 240 °C, and salinities between 11.8 and 13.4 wt.% $NaCl_{equiv}$ (Fig. 11b, App. 2). A single measurement (outlier) showed a T_h of 101 °C and 10.4 wt.% $NaCl_{equiv}$ salinity (Fig 11b, App. 2). The assemblage 517.1 from Gortavallig (Fig. 11b) shows the relatively highest T_h (239 to 271 °C) with low salinities (4.8 to 8.5 wt.% $NaCl_{equiv}$). The mean homogenization temperature T_h of all syn-Variscan fluid inclusion assemblages is 178 °C with a mean salinity of 10.2 wt.% $NaCl_{equiv}$ (n = 87).

Discussion

Basinal kinematics and fluid flow – N-S crustal extension provides E-W to ENE-WSW fluid pathways

The current study demonstrates that ore mineralization in SW Ireland shares a common structural regime to that described at Allihies on Beara Peninsula (Fig. 2; Lang *et al.* 2020). The kilometre scale E-W to ENE-WSW striking normal faults (Fig. 3) are part of the fault system that includes the basin controlling Coomnacronia-Killarney-Mallow Fault Zone and the Cork-Kenmare Fault Zone (Fig. 1; Naylor and Jones 1967; Capewell 1975; Price and Todd 1988; Meere 1995b; Vermeulen *et al.* 2000; Landes *et al.* 2003; MacCarthy 2007; Ennis *et al.* 2015; Lang *et al.* 2020). The large lateral extent of these faults onshore, as well as offshore (Fig. 3) suggest a deep-reaching fault system related to crustal extension (Fig. 12a; Naylor and Jones 1967). This corresponds with seismic interpretation from Landes *et al.* (2003) who determined a possible 13-14 km depth for the Cork-Kenmare Fault Zone. According to Williams *et al.* (1989) and Williams (2000) the E-W basinal faults show a steep dip to the South at Beara Peninsula and Sheep's Head (Fig. 12a+b); however, at Mizen Peninsula antithetic intrabasinal northwards dipping faults are inferred. The faults show an E-W strike at Beara Peninsula, Sheep's Head and northern Mizen Peninsula (Fig. 3), which rotates to an ENE-WSW strike on the south-western part of Mizen Peninsula. This rotation could be caused by a minor tectonic anticlockwise plate rotation during the basinal extension phase. Historically mined copper lodes (Fig. 3; Geological Survey Ireland Jetstream 2019) are related to these basin forming structures and their strike coincides with the regional orientation of these faults on the various West Cork peninsulas. Only a few historic copper lodes follow the kilometre scale N-S to NNE-SSW striking faults (Fig. 3). As one example Lang *et al.* (2020) described the large N-S lode at Mountain Mine, Allihies as a possible transfer fault or breached relay ramp (Walsh and Watterson 1991; Fossen and Rotevatn 2016). The large extent of these N-S faults can be explained by major cross-strike faults (Morley 1995) which are part of an extensional transfer fault system and can cut across multiple fault blocks. Sanderson (1984) noted N-S striking mineralized quartz veins on Beara Peninsula with strong folding and cleavage, which were interpreted as early extension veins.

On a local scale we see structures (Figs 4a, 5a, 6a, 7a, 8a, 9a), which show evidence for E-W to ENE-WSW striking extensional faults which are associated with meter-scale, steep dipping quartz veins and mineralized copper lodes. Stockwork-veining at Baurearagh (Fig. 4c) and hydraulic breccia with host rock sediment clasts within the quartz veins (Baurearagh, Fig. 4c and Caha Pass) indicate intensive hydrofracturing during pre-Variscan vein formation (Fig. 12a). The extensional phase caused a crustal thinning (Williams 2000), which resulted in a low lithostatic vs. hydrostatic ratio, which may have caused a rapid ascend of fluids in mobile hydrofractures (Bons 2001). These mobile hydrofractures can explain the large-scale vein precipitation. Large quartz veins are mainly concentrated into narrow zones (8 – 11 metres) of the outcrop adjacent to the extensional faults (e.g. Fig. 4a + 6a). The extensional faults, which provide the fluid pathways themselves were probably active for a longer time period which made them susceptible for surficial erosion.

Regional and microscopic evidence for a pre- and syn-Variscan mineralization

Some of the E-W/ENE-WSW striking faults with the associated mineralized quartz veins can show metre-scale folding (e.g. NW of Crookhaven, Fig. 8a). At the eastern end of the Gortavallig mine adits, the copper lode is described as “suddenly cut off” (Geological Survey Ireland, historic mine map 1863) which basically marks the reverse fault (Fig. 6a) caused by Variscan compression. Sinistral faulting of mineralized E-W veins has been described by Reilly (1986) occurring at Allihies and Mizen Peninsula (East) copper mines (Fig. 3). Syn-Variscan quartz veins were described at Allihies (Lang *et al.* 2020) as generally small-scaled (< 1 m) en echelon tension gashes in semi brittle shear zones. Generally, these syn-Variscan veins appear to be unmineralized. The WSW-ENE striking triangle zone at Dhurode (Figs 7a + 7b) also represents a Variscan feature. Similar structures can be found at Gortavallig (Fig. 6a) where the SW-NE striking syn-Variscan reverse fault shows no mineralization.

Microstructures and small-scale field observations support the premise of basin related extensional mineralization with a Variscan overprint. At Crookhaven the SW-NE striking quartz veins with splaying horsetail veinlets (Fig. 8b) indicate a local sinistral extensional movement (Fig. 3 + 8b). Several study localities from West Cork show cleavage within mineralization related E-W and ENE-WSW quartz veins ($S_{1,vein}$, e.g. Figs 8b and 8c). This veining cleavage ($S_{1,vein}$) represents a syn-compressional overprint. Similar to Allihies (Lang *et al.* 2020) a low angle of the vein's strike related to the Variscan NNW–SSE maximum principal stress σ1 forms the most distinct vein cleavage. Stylolites within the pre-Variscan quartz veins and mineralized lodes are very common (Figs 4f, 5b, 8f, 9d, 9e) and represent a weak form of cleavage (Alvarez *et al.* 1978) caused by pressure solution. Figure 5b shows that the stylolites are oriented normal to the NNW-SSE Variscan compression. Occasionally, the stylolites are rimmed by insoluble goethite (Fig. 8f) or molybdenite (Ballycummisk, Figs 9d + 9e). The goethite could be a remnant from altered sulfides within the quartz veins. Tectonism induced molybdenite stylolites have been described by Gaba (1990) and Lawley *et al.* (2013) occurring within other quartz vein related deposits.

The oriented sample of the mineralization related E-W striking quartz vein from Dhurode (Fig. 7c) has sweeping to patchy undulous extinction indicating a low-temperature crystal-plastic deformation (Trouw *et al.* 2009). The NNW-SSE striking microfault with partial recrystallization suggests low-grade sub-grain rotation during deformation (Fig. 7c: C+D; Trouw *et al.* 2009). The cataclastic fractured arsenopyrite from Gortavallig (Fig. 6d), the microfracture with altered bornite from Crookhaven (Fig. 8e) and the partially deformed hematite within the chalcopyrite from Ballycummisk (Fig. 9b) represent a post-mineralization semi-brittle deformation. Snodin (1972) described deformed chalcopyrite from the major quartz-sulfide veins e.g. Dhurode and Ballycummisk (Fig. 3) as clear evidence of intense deformation. This is in agreement with Meere (1995a, 1995b) who postulated a low-grade sub-greenschist-facies metamorphism during the Variscan Orogeny which caused an overprint to the major Cu mineralization at Allihies (Lang *et al.* 2020).

Syn-Variscan quartz veins are generally small scale (<1 m) and form stretched to fibrous antitaxial quartz fillings within tension gashes (Figs 4d + 6b). The crystals are typically formed during a continuous crack-seal event (Bons *et al.,* 2012). The mineralized sample from Crookhaven with fibrous kinked quartz and siderite crystals (Fig. 8g) also represents a continuous crack-seal event (Bons *et al.* 2012) generated by progressive deformation during the Variscan orogeny. The cleaved slate sample from Ballycummisk with the cross-cutting vein generations (Fig. 9f) represents an early, pre-compressional quartz precipitation, as well as a syn-compressional barite-quartz-hematite-chalcopyrite mineralization. This late mineralization took place after the major Variscan cleavage formation (Cooper and Trayner 1986; Ford 1987). From these observations it can be summarised that the second copper vein mineralization happened at the beginning of the Variscan Orogeny, and these veins were subsequently deformed by ongoing compression.

Fluid inclusions microthermometry of the pre-Variscan and syn-Variscan quartz veins

The fluid inclusion homogenization temperatures and salinities from the pre-Variscan E-W veins (Fig. 11a) display a range of T_h = 90° to 335 °C and 3.8 to 22.4 wt.% $NaCl_{equiv}$ which correspond with values observed at Allihies (Lang *et al.* 2020). The assemblages from the individual localities in West Cork were generally formed under quite similar T_h and salinity conditions (Fig. 11a, App. 2). Indeed, the different sample localities between each other show a wider spread in T_h and salinity (Fig. 11a, App. 2). This reflects the various and complex conditions with multiple fluid pulses which led to the primary mineralization in the Munster Basin. No sign of fluid mixing was recorded. Previous measurements from Dhurode, Crookhaven and Ballycummisk (Fig. 3; Wen *et al.* 1996) show T_h ranging between 100° and 348°C. Relatively high homogenization temperatures (Fig. 11a) are probably caused by crustal thinning during the extensional phase resulting high geothermal gradients (Meere 1995b; Williams 2000). Meere and Banks (1997) described comparable values but also showed a quartz vein from Allihies which has higher salinities (22-27 wt.% $NaCl_{equiv}$) than the results from this study (max. 22.4 wt.% $NaCl_{equiv}$). The high saline values were described by Lang *et al.* (2020) as localized assemblages from end members of a cooling fluid system occurring at the end of the primary mineralization phase. Carefully selected early inclusions do not show any sign of deformation or leaking during Variscan deformation.

Fluid inclusion assemblages in syn-Variscan samples from this study have a much narrower homogenization temperature and salinity range (T_h = 101 to 270 °C and 4.8 to 16.7 wt.% $NaCl_{equiv}$) than those from the pre-Variscan veins (Fig. 11b, App. 2). Lang *et al.* (2020) presented similar syn-Variscan homogenization temperatures from Allihies ranging between 121 and 243°C. In general, the syn-Variscan inclusions are less saline and show slightly cooler homogenization temperatures than the pre-Variscan inclusions.

Both vein types (pre-Variscan and syn-Variscan) display regional variations between sample localities (Fig. 11a and 11b). This suggests that the fluid is more affected by the different localities (e.g. minor host rock variations) and a similar fluid source generated both (pre- and syn-Variscan) mineral systems. Lower salinity and narrower T_h ranges imply evolving fluid pulses over time. The occurrences of siderite (Fig. 8g) and barite (Fig. 9b, 9c, 9f) at Crookhaven and Ballycummisk indicate that there are additional phases in the H_2O-NaCl fluid system. These are most likely $CaCl_2$ and $BaCl_2$. The H_2O–NaCl–$CaCl_2$-$BaCl_2$ system infers an early marine brine signature (Meere and Banks 1997). Downward migrating marine brines (Fig. 12a) at the end of the Devonian could well have triggered the early mineralization.

The Old Red Sandstone sediments of the Munster Basins are suitable as a possible metal source. The basinal sediment infill of over 6 km depth (Meere and Banks 1997) provides enough detrital material to function as copper source. According to Brown (2014) diagenetic pore waters can leach copper from labile minerals (e.g. pyroxenes, amphiboles, biotite, feldspars, magnetite) which are present in immature basin sediments. Large amounts of K-feldspar within the Munster Basin red bed sediments were identified by Meere et al. (2019).

Magmatism and mineralization

The molybdenite Re-Os model ages of 315.5 ± 1.6 Ma and 311.8 ± 1.6 Ma from Ballycummisk (Fig. 3; Table 3) coincide with the Ar/Ar phlogopite lamprophyric intrusion ages (314.44 ± 1.00 Ma; Quinn *et al.* 2005) from Black Ball Head near Allihies, and is supported by an Ar/Ar kaersutite age of 318 ± 3 Ma (Pracht and Timmerman 2004). These intrusions were formed during the early Variscan compression (Pracht and Kinnaird 1995; Pracht 2000). Coe (1959), Charlesworth (1963), Murphy (1960), and Fletcher (1969) presumed a magmatic intrusion as being the source for the sulfide mineralization. Nevertheless, no magmatic intrusion was dated in the time frame of the primary, pre-Variscan mineralization between 367.3 ± 5.5 and 366.4 ± 1.9 Ma (Allihies, Lang *et al.* 2020). None of the examined mineralized quartz veins in this study was directly or indirectly locally linked to a magmatic intrusion. Spinks *et al.* (2016) presented negative $\delta^{34}S_{CDT}$ values (-16.9 to -10.4 ‰) for chalcopyrite from Allihies. Wen *et al.* (1996) showed mostly negative $\delta^{34}S_{CDT}$ values (-21.0 to +5.1 ‰) for vein- and stratiform-disseminated deposits from West Cork. These negative values represent a bacteriogenic reduction of sulfur within the sediments and are evident for a sedimentary, non-magmatic fluid source. Higher fluid inclusion homogenization temperatures of up to 335 °C from Gortavallig or Ballycummisk Mines (Fig. 11) represent high geothermal gradients during basin formation (Meere 1995b; Williams 2000) with crustal thinning and upwelling of the Moho (Williams 2000).

Timing of the copper emplacement and previous mineralization models

According to Spinks *et al.* (2016) and Wen *et al.* (1996) the originally stratiform syngenetic-diagenetic sulfide mineralization was remobilized by metamorphic fluids into quartz veins at different stages of the Variscan Orogeny. Meere and

Banks (1997) associated minor vein formation with the early Variscan compression. All three studies (Wen *et al.* 1996, Meere and Banks 1997, Spinks *et al.* 2016) defined the major vein formation as a post-Variscan N-S oriented relaxation event.

The demonstrated outcome of this study, as well as recent structural observations from Lang *et al.* (2020) show that the major E-W to ENE-WSW vein-hosted Cu mineralization is related to early basinal extension and pre-dates the Variscan Orogeny. This early mineralization is followed by a second syn-compressional event. In the following paragraph we provide new constraints on the timing of these two events:

The copper deposits from Allihies (Fig. 3) show an age between 367.3 ± 5.5 and 366.4 ± 1.9 Ma (Re-Os; Lang *et al.* 2020) and are described as syn-basinal mineralization during the Famennian Stage (Cohen *et al.* 2023) of the Upper Devonian. The second episode of Cu-vein formation is related to the early compressional phase at Ballycummisk (Fig. 3) between 315.5 ± 1.6 Ma and 311.8 ± 1.6 Ma (molybdenite Re-Os model ages, Table 3) belonging to the Bashkirian to Moscovian Stage (Cohen *et al.* 2023) of the Pennsylvanian (Upper) Carboniferous. The molybdenite stylolitisation at Ballycummisk (Figs 9d + 9e) indicates that the samples suffered compressional deformation. According to Stein *et al.* (2001) the molybdenite still represents the primary mineralization, as the Re-Os chronometer is resistant to high-grade metamorphism and deformation. As the dated molybdenite is syngenetically intergrown with chalcopyrite (Fig. 9c), it is reasoned that the Re-Os ages represent the major Cu emplacement at Ballycummisk. Based on Ar-Ar dates of deformed intrusive rocks on Beara Peninsula Quinn *et al.* (2005) postulated that the initial effect of the Variscan compression with cleavage formation started before 314.4 Ma which indicates that the compressional mineralization was emplaced after the beginning of the Variscan Orogeny.

This newly classified time-setting of a syn-basinal and an early Variscan mineralization phase contradicts the previous mineralization models which presumed a post-Variscan emplacement by metamorphic fluids (Wen *et al.* 1996; Meere and Banks 1997; Spinks *et al.* 2016). The erroneously interpreted post-Variscan quartz vein (copper lode) formation can be explained by the structural nature of the quartz veins themselves. The massive, sometimes metre-wide quartz veins are very competent while host rock sediments (mostly sandstones and siltstones) are less incompetent and show strong cleavage and folding. At first glance it appears that the E-W striking quartz veins postdate the Variscan compression and crosscut the deformed basin sediments. Cleavage, minor folding and faulting of the quartz veins can be easily overlooked or misinterpreted as surficial weathering.

As mentioned before, the early Variscan Cu mineralization at Ballycummisk took place *after* the major Variscan cleavage formation (Fig. 9f; Cooper and Trayner 1986; Ford 1987), but still relatively early in the Variscan deformation cycle. The cleavage formation provided fractures within the pre-Variscan basinal mineralized quartz veins (e.g. Fig. 9f). These cleavage related pathways allowed a sulfide remobilization by low-grade sub-greenschist-facies metamorphic fluids (Meere 1995a, 1995b). As described by Spinks *et al.* (2016) the metamorphic fluids were responsible for remobilising both sulfur and metals. The relatively low solubility of 0.01 ppm metals (e.g. copper) requires a sulfide-rich source (e.g. early pre-Variscan veins) and/or a high fluid flow under low pH conditions. The early Variscan reactivation of pre-Variscan mineralized basinal fault systems provided an immediately adjacent sampling and sulfide remobilization from the early into the late Cu-vein systems over a very short distance. Both mineralization generations show therefore a highly proximal emplacement.

Sediment-hosted stratiform copper (SSC) deposits and exploration potential

Sediment-hosted stratigraphically bound copper mineralization within the Munster Basin was described by Snodin (1972) and Wen *et al.* (1996). The disseminated copper mineralization occurs in reduced green sandstone zones (green beds, transition zone) within the upper Castlehaven Formation just below the nonreddish Toe Head Formation (see Fig. 2b). The typical SSC deposits, such as the Permian Kupferschiefer in Germany and Poland and the Zambian Central African Copperbelt have a sedimentary basin architecture with continental siliciclastic sedimentary rocks (red beds) which are overlain by nonreddish siltstones, sandstones, carbonates and/or shales, known as reduced graybeds (e.g. Kirkam 1989; Hitzman *et al.* 2005; Brown 2014 and references herein). In SSC deposits the reduced graybeds form a stratiform thin-layered host rock for the sulfide mineralization (Hitzman *et al.* 2005). The observations of this study show that the vein hosted copper deposits of West Cork are predominantly hosted within sandstone and siltstone formations of the oxidized Upper Devonian siliciclastic sediments (Fig. 12a). Only with regard to the host lithology of an SSC type deposit the copper mineralization of the Muster Basin in West Cork could be classified as a Redbed-Type Copper Deposit which is generally hosted by the oxidized red bed sequence and not by the reduced graybeds (Brown 2014). Examples include Dzhezkazgan in Kazakhstan and Lisbon Valley in Utah (Brown 2014; Hitzman *et al.* 2005). The copper mineralization in SSC deposits is often related to organic matter; for example, pyritized plant debris is replaced by copper sulfides (e.g. Cumberland Basin of Nova Scotia; Brown 2014). The cellular permineralized plant fossil from Killeen North (Figs 3 + 6h) is a nice example for this sediment hosted copper mineralization. The sample was found next to a historically mined E-W lode. Therefore, it is suspected that this Cu fossilisation is in direct relation to the pre-Variscan basinal vein mineralization. Cu- and S-rich fluids possibly percolated from the extensional faults into the highly porous host rock conglomerates and replaced the organic cellular material by redox reaction (e.g. Berner 1984). Comparable to this is the occurrence of disseminated chalcopyrite within an organic-rich slate next to a mineralized quartz vein from Gortavallig (Fig. 6g). The mineralized siltstone next to the chalcopyrite-rich quartz vein from Crookhaven (Fig. 8d) provides another similar example. Apart from these examples the sulfide mineralization of the examined localities is mainly hosted within the quartz veins. This is not typical for a sediment-hosted stratiform copper deposit. Vein-style mineralization can occur for example at the Kupferschiefer Deposit in Poland/Germany or at Coates Lake Deposit in Canada but is generally subordinate and the veins are rather described as veinlets (<1 to 15 cm; Hitzman *et al.* 2005; Milton *et al.* 2017). The examined deposits of West Cork could be named as <u>vein hosted</u> Redbed-Type SSC deposits.

Comparison with Zn-Pb Deposits of the Irish Midlands

The Cu mineralization in the SW Ireland was compared with the large Zn-Pb deposits of the Irish Midlands. Pyrite Re-Os dates reveal an age of 346.6 ± 3.0 Ma at Lisheen and 334.0 ± 6.1 Ma at Silvermines (Hnatyshin *et al.* 2015). This postdates the mineralization at Allihies (367.3 ± 5.5 and 366.4 ± 1.9 Ma) but predates the ages from Ballycummisk (315.5 ± 1.6 Ma and 311.8 ± 1.6 Ma). Similarities of the examined localities in West Cork to the Irish Midlands can be observed in the geostructural genesis and kinematics of the deposits. Comparable to the observations in this study, Silvermines and Tynagh Mine are related to E-W striking normal faults, caused by a pre-Variscan N-S extensional phase (e.g. Kinnaird *et al.* 2002; Hitzman 1999). In contrary to the mainly siliciclastic (Upper Devonian) hosted West Cork deposits Navan, Lisheen, Galmoy, Silvermines and Tynagh are hosted within the Lower Carboniferous carbonates next to the E-W and SW-NE faults (e.g. Gleeson and Yardley 2002 and Everett *et al.* 1999b). Late Carboniferous Variscan reactivation of normal faults and the formation of transpressional faults in the Irish Midlands (Coller 1984; Johnston *et al.* 1996; Hitzman 1999; Kyne *et al.* 2017; Torremans *et al.* 2018) can be compared with reactivated faults at Baurearagh (Tab. 1), the compressional mineralized quartz vein from Crookhaven (Fig. 8g) and the early Variscan mineralized veins from Ballycummisk (Fig. 9f).

Fluid inclusion measurements from the Irish Type Deposits show a range of up to about 240°C for homogenization temperature and low salinities (about 10 wt% $NaCl_{equiv}$), to very low T_h values with a minimum of about 55°C and a high salinity of up to 24 wt% $NaCl_{equiv}$ (Wilkinson 2001, 2010; Gleeson and Yardley 2002). Banks (2002) interpreted from chloride and Br concentrations (crush + leach studies), that the main ore fluid from Tynagh and Silvermines was seawater that had evaporated until the salinity was between 12 and 18 wt%. Measurements from pre-Variscan E-W veins of West Cork (Fig. 11a) indicate comparable values, but homogenization temperatures T_h can get hotter with up to 335 °C and the salinity can show even lower concentrations with 5.2 wt% $NaCl_{equiv}$.

Conclusions

(1) Copper mineralization in West Cork is predominantly related to extensional E-W to ENE-WSW striking basin structures, which form pathways for deep sourcing metal-rich fluids. The ore is often hosted within large meter- to tens of meters-scale quartz veins with occasional high-pressure hydraulic brecciation and stockwork veining. Sediment-hosted mineralization related to the extensional basin structures is also present as fluids can perculate into unconsolidated sediments nearby the fault systems. All E-W quartz veins and extensional structures show a Variscan compressional overprint (folding, cleavage, stylolitisation, brecciation), whereby a reverse reactivation of the extensional fractures is possible, and Cu mineralization was emplaced during early compressional phase. Pre-Variscan, mineralizing fluid inclusion assemblages show multiple fluid pulses with homogenization temperatures T_h from 90 to 335 °C. Salinities vary between 3.8 and 22.4 wt% $NaCl_{equiv}$. Syn-Variscan quartz veins show also multiple pulses with T_h ranges from 101 to 270 °C and with salinities between 4.8 and 16.7 wt% $NaCl_{equiv}$. There is no evidence for a magmatic driven fluid source. The Old Red Sandstone sediments within the Munster Basins are a possible metal source.

(2) The timing of Cu mineralization (molybdenite Re-Os) reveals two distinct episodes from primary syn-basinal formation at Allihies between 367.3 ± 5.5 and 366.4 ± 1.9 Ma, to an early compressional phase with remobilisation (secondary episode) at Ballycummisk between 315.5 ± 1.6 Ma and 311.8 ± 1.6 Ma.

(3) The basin architecture of the West Cork copper mineralization shows genetic links to the Redbed-Type SSC deposits and a structural kinematic similarity to the Zn-Pb deposits of the Irish Midlands. A focus

for successful mineral exploration in this area or tectonically similar basin structures should be the syn-basinal extensional fault systems as they provide the primary pathway for mineralizing fluids which can form vein hosted and sediment hosted Cu deposits. Reactivated extensional fault systems owing to tectonic inversion can cause a remobilisation and reconcentration of valuable mineralization.

Acknowledgements

This publication has emanated from research supported in part by a research grant from Science Foundation Ireland (SFI) under Grant Number 13/RC/2092 and is co-funded under the European Regional Development Fund and by iCRAG industry partners.

The authors are grateful for the field, laboratory and software assistance from Ronan Hennessy (University College Cork), Chris Ottley and Geoff Nowell (Durham University). Many thanks to the local residents from Crookhaven Peninsula for granting access to the historic mining sites. Special thanks to the National History Museum in London (Simon Kocher and Robin Hansen) for providing molybdenite sample material (BM.1964,R230) from the historic Russell collection.

The Geological Survey Ireland are acknowledged for providing regional data and background information for our 2-D mapping and 3-D modelling efforts. We also thank ARANZGeo/Seequent (Leapfrog3DGeo), Emerson Paradigm (SKUA-GoCAD), Microsoft (Bing Satellite Maps, 2016-2019), Google Maps (2016-2019), Mira Geoscience (Mining Suite Plugins), Modri planet d.o.o. (3Dsurvey) and ESRI (ArcGIS) for providing support and academic licenses of software essential to this project.

References

Allmendinger, R.W., Cardozo, N.C., and Fisher, D., 2013, Structural Geology Algorithms: Vectors & Tensors. Cambridge University Press, Cambridge.
Atkinson, Jr. A.B., 2002. A Model for the PTX Properties of H2O–NaCl: MSc thesis, Virginia Tech, Blacksburg, VA.

Alvarez, W., Engelder, T., and Geiser, P.A., 1978, Classification of solution cleavage in pelagic limestones: Geology, v. 6(5), p. 263-266, doi: 10.1130/0091-7613(1978)6<263:COSCIP>2.0.CO;2.

Atkinson, Jr. A.B., 2002, A Model for the PTX Properties of H2O–NaCl: MSc thesis, Virginia Tech, Blacksburg, VA.

Banks, D.A., Boyce, A.J., and Samson, I.M., 2002, Constraints on the origins of fluids forming Irish Zn-Pb-Ba deposits: Evidence from the composition of fluid inclusions: Economic Geology and the Bulletin of the Society of Economic Geologists, v. 97(3), p. 471-480.

Berner, R.A., 1984, Sedimentary pyrite formation: An update: Geochimica et Cosmochimica Acta, v. 48(4), p. 605-615, doi: 10.1016/0016-7037(84)90089-9.

Bodnar, R.J., 1983, A method of calculating fluid inclusions volumes based on vapor bubble diameters and P–V–T–X properties of inclusion fluids: Economic Geology, v. 78, p. 535–542, doi: 10.2113/gsecongeo.78.3.535.

Bodnar, R.J., 1993, Revised equation and table for determining the freezing point depression of H2O–NaCl solutions: Geochimica et Cosmochimica Acta, v. 57, p. 683–684, doi: 10.1016/0016-7037(93)90378-A.

Bodnar, R.J., and Vityk, M.O., 1994, Interpretation of microthermometric data for H2O–NaCl fluid inclusions, *in* Vivo, B.D. and Frezzotti, M.L., eds., Fluid

Inclusions in Minerals, Methods and Applications: Virginia Tech, Blacksburg, VA, p. 117–130.

Boldy, G.D.J., 1955, The Petrology of the Igneous rocks near Castletownbere, West Co. Cork and their relationship with the Armorican Orogenesis in S.W. England: Unpublished M.Sc. Thesis, Trinity College, Dublin.

Bons, P., 2001, The formation of large quartz veins by rapid ascent of fluids in mobile hydrofractures: Tectonophysics, v. 336, p. 1-17, doi: 10.1016/S0040-1951(01)00090-7.

Bons, P.D., Elburg, M., and Gomez-Rivas, E., 2012, A review of the formation of tectonic veins and their microstructures: Journal of Structural Geology, v. 43, p. 33–62, doi: 10.1016/j.jsg.2012.07.005.

Brown, A.C., 2014, Low-Temperature Sediment-Hosted Copper Deposits, *in* Heinrich, D., Holland, Karl, Turekian, K., eds., Treatise on Geochemistry (Second Edition): Elsevier, p. 251-271, doi: 10.1016/B978-0-08-095975-7.01110-4.

Capewell, J., 1975, The Old Red Sandstone Group of Iveragh, Co. Kerry: Proceedings of the Royal Irish Academy, Section B, v. 75, p. 155–171.

Cardozo, N., and Allmendinger, R. W., 2013, Spherical projections with OSXStereonet: Computers & Geosciences, v. 51(0), p. 193-205, doi: 10.1016/j.cageo.2012.07.021.

Caumon, G., Collon-Drouaillet, P., Le Carlier de Veslud, C., Viseur, S., and Sausse, J., 2009, Surface-based 3-D modelling of geological structures: Mathematical Geosciences, v. 41, p. 927–945, doi: 10.1007/s11004-009-9244-2.

Charlesworth, J.K., 1963, Historical Geology of Ireland. Oliver and Boyd, 565 p.

Cohen, K.M., Finney, S.C., Gibbard, P.L. & Fan, J.-X. (2023; updated) The ICS International Chronostratigraphic Chart. Episodes 36: 199-204, International Commission on Stratigraphy, IUGS (www.stratigraphy.org).

Coe, K., 1959, Intrusion breccia of Dunmore, Co. Donegal. Geol. Mag., v. 96, p. 172-173.

Coller, D.W., 1984, Variscan structures in the Upper Palaeozoic rocks of west central Ireland: Geological Society, London, Special Publications, v. 14, p. 185–194, doi: 10.1144/GSL.SP.1984.014.01.18.

Cooper, M.A., and Trayner, P.M., 1986, Thrust-surface geometry: implications for thrust-belt evolution and section-balancing techniques: Journal of Structural Geology, v. 8, p. 305–312, doi: 10.1016/0191-8141(86)90051-9.

Doppler, G., Bakker, R.J., 2014, The influence of the α–β phase transition of quartz on fluid inclusions during re-equilibration experiments: Lithos, v. 198–199, p. 14–23.

Duffy, T.J., 1932, Copper Deposits in Southwest Ireland: Unpublished report and field sheets. Geol. Surv. Ireland.

Ennis, M., Meere, P.A., Timmerman, M.J., and Sudo, M., 2015, Post-Acadian sediment recycling in the Devonian Old Red Sandstone of Southern Ireland: Gondwana Research, v. 28, p. 1415–1433, doi: 10.1016/j.gr.2014.10.007.

ESRI, ArcGIS, 2019, Esri, DigitalGlobe, GeoEye, Earthstar Geographics, CNES/Airbus DS, USDA, USGS, AeroGRID, IGN, and the GIS User Community

Everett, C.E., Wilkinson, J.J., and Rye, D.M., 1999b, Fracture-controlled fluid flow in the Lower Palaeozoic basement rocks of Ireland: Implications for the genesis of Irish-type Zn-Pb deposits, *in* McCaffrey, K.J.W., Lonergan, L. & Wilkinson, J.J., eds., Fractures, Fluid Flow and Mineralization: Geol. Soc. Spec. Pub., v. 155, p. 247-276.

Fletcher, C.I., 1969, The sulphide mineralization in the Allihies region, County Cork, Eire: Ph.D. Dissertation, University of Leicester, p. 128–129.

Ford, M., 1987, Practical application of the sequential balancing technique: an example from the Irish Variscides: Journal of the Geological Society, London, v. 144, p. 885–891, doi: 10.1144/gsjgs.144.6.0885.

Fossen, H., and Rotevatn, A., 2016, Fault linkage and relay structures in extensional settings – A review: Earth-Science Reviews, v. 154, p. 14–28, doi: 10.1016/j.earscirev.2015.11.014.

Gaba, R.G., 1990, Stockwork Molybdenite in the Mission Ridge Pluton: A new Exploration Target in the Bridge River Mining Camp* (92J/16): British Columbia Geological Survey Branch, Geological Fieldwork IYR9, Paper 1990-1.

Geological Survey of Ireland, GSI, unknown author, 1863, Gortavallig Mine, Horizontal Plan: GSI Goldmine (https://secure.dccae.gov.ie/goldmine/docpage.html?id1=8260692&id2=9553735&id3=9557012).

Geological Survey of Ireland, GSI, 2016, Bedrock 100k (scale 1:100,000), Bedrock Geology, Coordinate System: Irish Transverse Mercator / ITM (https://www.gsi.ie/en-ie/data-and-maps/Pages/Bedrock.aspx#).

Geological Survey of Ireland, GSI Infomar, 2017, Bathymetry - South West - bylrsw10m. INFOMAR INSS 10m Bathymetry & LIDAR WGS84 projection. Ireland. LAT (lowest astronomical tide), (https://www.infomar.ie/data/)

Geological Survey of Ireland, GSI Jetstream, 2019, Historical Maps of Copper Deposits in SW Ireland (https://jetstream.gsi.ie)

Gleeson, S.A., and Yardley, B.W.D., 2002, Extensional Veins and Pb–Zn Mineralisation in Basement Rocks: The Role of Penetration of Formation Brines, *in* Stober, I., and Bucher, K., eds., Water–Rock Interaction. Water Science and Technology Library, Vol. 40: Springer, Dordrecht, p. 189–205.

Goldstein, R.H., and Reynolds, T.J., 1994, Systematics of fluid inclusions in diagenetic minerals: SEPM (Society for Sedimentary Geology), USA

Halliday, A.N., and Mitchell, J.G., 1983, K–Ar ages of clay concentrates from Irish orebodies and their bearing on the timing of mineralisation: Earth and Environmental Science Transactions of the Royal Society of Edinburgh, v. 74, p. 1–14, doi: 10.1017/S0263593300009858.

Hitzman, M.W., 1999, Extensional faults that localize Irish syndiagenetic Zn–Pb deposits and their reactivation during Variscan compression: Geological Society, London, Special Publications, v. 155, p. 233–245, doi: 10.1144/GSL.SP.1999.155.01.17.

Hitzman, M.W., Kirkham, R., Broughton, D., Thorson, J., and Selley, D., 2005, The sediment hosted stratiform copper ore system, *in* Hedenquist, J.W., Thompson, J.F.H., Goldfarb, R.J., and Richards, J.P., eds., Economic Geology 100th Anniversary Volume 1905–2005: Littleton, CO, Society of Economic Geologists, Inc. p. 609–642.

Hnatyshin, D., Creaser, R.A., Wilkinson, J.J., and Gleeson, S.A., 2015, Re–Os dating of pyrite confirms an early diagenetic onset and extended duration of mineralization in the Irish Zn–Pb ore field: Geology, v. 43, p. 143–146, doi:10.1130/G36296.1.

Jarvis, A., Reuter, H.I., Nelson, A., and Guevara, E., 2008, Hole-filled SRTM for the globe Version 4: International Centre for Tropical Agriculture (CIAT), (http://srtm.csi.cgiar.org).

Johnston, J.D., Coller, D., Millar, G., and Critchley, M.F., 1996, Basement structural controls on Carboniferous-hosted base metal mineral deposits in Ireland: Geological Society, London, Special Publication, v. 107, p. 1-21.

Kinnaird, J.A., Ixer, R.A., Barreiro, B., and Nex, P.A., 2002, Contrasting sources for lead in Cu-polymetallic and Zn–Pb mineralisation in Ireland: constraints from lead isotopes: Mineralium Deposita, v. 37, p. 495–511, doi: 10.1007/s00126-001-0252-5.

Kirkham, R.V., 1989, Distribution, setting and genesis of sediment-hosted stratiform copper deposits, *in* Boyle, R.W., Brown, A.C., Jefferson, C.W., Jowett, E.C., and Kirkham, R.V., eds., Sediment-Hosted Stratiform Copper Deposits, Geological Association of Canada Special Paper 36: Ottawa, Geological Association of Canada, p. 3–38.

Kocianova, L., 2016, Orientation Analysis Tools for ArcGIS: OATools (https://is.muni.cz/www/lenka.koc/prvnistrana.html).

Kyne, R., Torremans, K., Güven, J., Doyle, R., and Walsh, J., 2017, 3-D Modeling of the Lisheen and Silvermines Deposits, County Tipperary, Ireland: Insights into Structural Controls on the Formation of Irish Zn-Pb Deposits: Economic Geology, v. 114 (1), p. 93-116, doi: 10.5382/econgeo.2019.4621.

Landes, M., O'Reilly, B.M., Readman, P.W., Shannon, P.M., and Prodehl, C., 2003, VARNET-96: three-dimensional upper crustal velocity structure of SW Ireland: Geophysical Journal International, v. 153, p. 424–442, doi: 10.1046/j.1365-246X.2003.01911.x.

Lang, J., Meere, P. A., Unitt, R. P., Johnson, S. C., Solferino, G., Torremans, K., Selby, D., and Kyne, R., 2020, The Vein Hosted Copper Deposits of the Allihies Mining Area, Southwest Ireland – A New Structural and Chronological Evaluation: Journal of the Geological Society, v. 177, p. 671-685, doi: 10.1144/jgs2019-154.

Lawley, C., Selby, D., and Imber, J., 2013, Re-Os Molybdenite, Pyrite, and Chalcopyrite Geochronology, Lupa Goldfield, Southwestern Tanzania: Tracing Metallogenic Time Scales at Midcrustal Shear Zones Hosting Orogenic Au Deposits: Economic Geology, v. 108, p. 1591-1613, doi: 10.2113/econgeo.108.7.1591.

Li, Y., Selby, D., Condon, D., and Tapster, S., 2017, Cyclic Magmatic–Hydrothermal Evolution in Porphyry Systems: High-Precision U–Pb and Re–Os Geochronology Constraints on the Tibetan Qulong Porphyry Cu–Mo Deposit: Economic Geology, v. 112, p. 1419–1440, doi: 10.5382/econgeo.2017.4515.

MacCarthy, I.A.J., 1990, Alluvial sedimentation patterns in the Munster Basin, Ireland: Sedimentology, v. 37, p. 685–712, doi: 10.1111/j.1365-3091.1990.tb00629.x.

MacCarthy, I.A.J., 2007, The South Munster Basin of southwest Ireland: Journal of Maps, v. 3, p. 149–172, doi: 10.1080/jom.2007.9710835.

MacCarthy, I.A.J., Pracht, M., and Sleeman, A.G., 2002, Geology of West Cork, Scale 1:100000, Sheet 24: Geological Survey of Ireland, Dublin.

Meere, P.A., 1995a, High and low density fluids in a quartz vein from the Irish Variscides: Journal of Structural Geology, v. 17, p. 435–446, doi: 10.1016/0191-8141(94)00066-9.

Meere, P.A., 1995b, Sub-greenschist facies metamorphism from the Variscides of SW Ireland an early syn-extensional peak thermal event:

Journal of the Geological Society, London, v. 152, p. 511–521, doi: 10.1144/gsjgs.152.3.0511.

Meere, P.A., 1995c, The structural evolution of the western Irish Variscides: an example of obstacle tectonics?: Tectonophysics, v. 246, p. 97–112, doi: 10.1016/0040-1951(94)00267-D.

Meere, P.A., and Banks, D.A., 1997, Upper crustal fluid migration: an example from the Variscides ofSW Ireland: Journal of the Geological Society, London, v. 154, p. 975–985, doi: 10.1144/gsjgs.154.6.0975.

Milton, J.E., Hickey, K.A., Gleeson, S.A., Falck, and H., Allaz, J., 2017, In Situ Monazite Dating of Sediment-Hosted Stratiform Copper Mineralization in the Redstone Copper Belt, Northwest Territories, Canada: Cupriferous Fluid Flow Late in the Evolution of a Neoproterozoic Sedimentary Basin: Economic Geology, v. 112 (7), p. 1773–1806. doi: 10.5382/econgeo.2017.4529.

Montañez, I. P., and Crossey, L., J., 2017, Diagenesis: Encyclopedia of Engineering Geology, v. 1–11. doi: 10.1007/978-3-319-39193-9_35-1.

Morley, C.K., 1995, Developments in the structural geology of rifts over the last decade and their impact on hydrocarbon exploration: Geological Society, London, Special Publications, v. 80, p. 1-32, doi: 10.1144/GSL.SP.1995.080.01.01.

Murphy, T., 1960, Gravity Anomaly Maps of Ireland, Sheet 5 - south-west. Communications of the Dublin Institute for Advanced Studies, Geophysical Bulletin no. 18.

Naylor, D., and Jones, P.C., 1967, Sedimentation and tectonic setting of the Old Red Sandstone of southwest Ireland, *in* Oswald, D., ed., International Symposium on the Devonian System (Calgary). Society of Petroleum Geology 2: Calgary, Alberta, p. 1089–1099.

Naylor, D., Higgs, K. and Boland, M.A., 1977, Stratigraphy on the North Flank of the Dunmanus Syncline, West Cork. Bulletin of the Geological Survey of Ireland, v. 2, p. 143-157.

Naylor, D., Reilly, T.A., Sevastopulo, G.D. and Sleeman, A.G., 1983, Stratigraphy and Structure in the Irish Variscides. *in* Hancock, P., ed., The Variscan Fold Belt. Adam Huger Ltd., Bristol, v. 2, p. 1-46.
O'Brien, M.V., 1959, The future of non-ferrous mining in Ireland, *in* Jones, W. R., Bates, C. P., and Charles, A. G., eds., The Future of Non-Ferrous Mining in Great Britain and Ireland: Institution of Mining and Metallurgy Symposium, p. 5–26.

O'Brien, W.F., 1987, The dating of the Mt Gabriel-type copper mines of West Cork: Journal of the Cork Historical and Archaeological Society, v. 92, p. 50–70.

Pracht, M., 2000, Controls on magmatism in the Munster Basin, SW Ireland: Geological Society, London, Special Publications, v. 180, p. 303–317, doi: 10.1144/GSL.SP.2000.180.01.14.

Pracht, M., and Kinnaird, J.A., 1995, Mineral chemistry of megacrysts and ultramafic nodules from an undersaturated pipe at Black Ball Head, County Cork: Irish Journal of Earth Sciences, v. 14, p. 47–58.

Pracht, M., and Kinnaird, J., 1997, Carboniferous subvolcanic activity on the Beara Peninsula, SW Ireland. Geological Journal. V. 32 p. 297 – 312, doi: 10.1002/(SICI)1099-1034(199712)32:4<297::AID-GJ736>3.0.CO;2-X.

Pracht, M., and Sleeman, A.G., 2002, A geological description of West Cork and adjacent parts of Kerry to accompany the Bedrock Geology, 1:100,000 Scale Map Series, Sheet 24, West Cork. With accompanying contributions by Wright G (Groundwater) and CoxW (Minerals): Geological Survey of Ireland, Dublin.

Pracht, M., and Timmerman, M., 2004, A Late Namurian (318Ma) 40Ar/39Ar Age For Kaersutite Megacrysts from the Black Ball Head Diatreme: an Age Limit for the Variscan Deformation in South-West Ireland. Irish Journal of Earth Sciences, v. 22, p. 35-45 doi: 10.3318/IJES.2004.22.1.33.

Price, C.A., and Todd, S.P., 1988, A model for the development of the Irish Variscides: Journal of the Geological Society, London, v. 145, p. 935–939, doi: 10.1144/gsjgs.145.6.0935.

Quinn, D., Meere, P.A., and Wartho, J.A., 2005, A chronology of foreland deformation: Ultra-violet laser 40Ar/39Ar dating of syn/late-orogenic intrusions from the Variscides of southwest Ireland: Journal of Structural Geology, v. 27, p. 1413–1425, doi: 10.1016/j.jsg.2005.02.003.

Reilly, T.A., 1986, A review of vein mineralization in SW County Cork, Ireland, *in* Andrew, C.J., Crowe, R.W.A., Finlay, S., Pennell, W.M., and Pyne, J.F., eds., Geology and Genesis of Mineral Deposits in Ireland: Irish Association for Economic Geology, Dublin, p. 513–544.

Sanderson, D.J., 1984, Structural variation across the northern margin of the Variscides in NW Europe: Geological Society, London, Special Publications, v. 14, p. 149–165, doi: 10.1144/GSL.SP.1984.014.01.15.

Selby, D., and Creaser, R.A., 2001, Re–Os geochronology and systematics in molybdenite from the Endako porphyry molybdenum deposit, British Columbia, Canada: Economic Geology, v. 96, p. 197–204, doi: 10.2113/gsecongeo.96.1.197.

Selby, D., Creaser, R.A., Stein, H.J., Markey, R.J., and Hannah, J.L., 2007, Assessment of the 187Re decay constant by cross calibration of Re–Os molybdenite and U–Pb zircon chronometers in magmatic ore systems: Geochimica et Cosmochimica Acta, v. 71, p. 1999–2013, doi: 10.1016/j.gca.2007.01.008.

Sheridan, D.J., 1964, The structure and mineralisation of the Mountain Mine area, Allihies, west Co. Cork, Ireland: Scientific Proceedings, Royal Dublin Society, Series A, v. 2, p. 21–27.

Smoliar, M.I., Walker, R.J., and Morgan, J.W., 1996, Re–Os ages of group IIA, IIIA, IVA, and IVB iron meteorites: Science, v. 271, p. 1099–1102, doi: 10.1126/science.271.5252.1099.

Snodin, S.R., 1972, Copper and other mineralisation in the Upper Palaeozoic strata of south-west Cork, Ireland, and related areas: Unpublished Ph.D. Thesis. University of Leicester.

Spinks, S.C., Parnell, J., Bellis, D., and Still, J., 2016, Remobilization and mineralization of selenium–tellurium in metamorphosed red beds: Evidence from the Munster Basin, Ireland: Ore Geology Reviews, v. 72, p. 114–127, doi: 10.1016/j.oregeorev.2015.07.007.

Steele-MacInnis, M., Bodnar, R.J., and Naden, J., 2011, Numerical model to determine the composition of H2O–NaCl–CaCl2 fluid inclusions based on microthermometric and microanalytical data: Geochimica et Cosmochimica Acta, v. 75, p. 21–40, doi: 10.1016/j.gca.2010.10.002.

Steele-MacInnis, M., Lecumberri-Sanchez, P., and Bodnar, R.J., 2012, Short note: HokieFlincs_H2O-NaCl: A Microsoft Excel spreadsheet for interpreting microthermometric data from fluid inclusions based on the PVTX properties of H2O–NaCl: Computers & Geosciences, v. 49, p. 334–337, doi: 10.1016/j.cageo.2012.01.022.

Stein, H.J., Markey, R.J., Morgan, J.W., Hannah, J.L., and Scherstén, A., 2001, The remarkable Re-Os chronometer in molybdenite: How and why it works: Terra Nova, v. 13, p. 479-486, doi: 10.1046/j.1365-3121.2001.00395.x.

Torremans, K., Kyne, R., Doyle, R., Güven, J.F., and Walsh, J.J., 2018, Controls on Metal Distributions at the Lisheen and Silvermines Deposits: Insights into Fluid Flow Pathways in Irish-Type Zn-Pb Deposits: Economic Geology, v. 113 (7), p. 1455-1477, doi: 10.5382/econgeo.2018.4598.

Trouw, R.A.J., Passchier, C.W., and Wiersma, D.J., 2009, Crystal-Plastic Deformation, Recovery and Recrystallisation of Quartz, *in* Atlas of Mylonites and Related Microstructures: Springer, Berlin, p. 241–262.

Vermeulen, N.J., Shannon, P.M., Masson, F., and Landes, M., 2000, Wide-angle seismic control on the development of the Munster Basin, SW Ireland: Geological Society, London, Special Publications, v. 180, p. 223–237, doi: 10.1144/GSL.SP.2000.180.01.11.

Viswanathiah, M.N., 1959, Geology and Mineralisation around Allihies – Castletownbere Area. Co. Cork, Ireland: Unpublished Ph.D. Thesis, London University.

Walsh, J.J., and Watterson, J., 1991, Geometric and kinematic coherence and scale effects in normal fault systems: Geological Society, London, Special Publications, v. 56, p. 193–203, doi: 10.1144/GSL.SP.1991.056.01.13.

Wen, N., Boyce, A.J., Fallick, A.E., Ashworth, J.R., and Ixer, R.A., 1996, The genesis of Cu-bearing quartz veins by metamorphic remobilization from stratiform red bed deposits, SW County Cork, Ireland: Mineralogy and Petrology, v. 57, p. 73–89, doi: 10.1007/BF01161622.

Wilkinson, J.J., 2001, Fluid inclusions in hydrothermal ore deposits: Lithos, v. 55, p. 229–272, doi: 10.1016/S0024-4937(00)00047-5.

Wilkinson, J.J., 2010, A Review of Fluid Inclusion Constraints on Mineralization in the Irish Ore Field and Implications for the Genesis of

Sediment-Hosted Zn–Pb Deposits: Economic Geology, v. 105, p. 417–442, doi: 10.2113/gsecongeo.105.2.417.

Williams, R.A., 1991, The Berehaven copper mines: British Mining, v. 42. Northern Mine Research Society, Sheffield.

Williams, E.A., Bamford, M.L.F., Cooper, M.A., Edwards, H.E., Ford, M., Grant, G.G., MacCarthy, I.A.J., McAfee, A.M., and O'Sullivan, M.J., 1989, Tectonic controls and sedimentary response in the Devonian-Carboniferous Munster and South Munster basins, south-west Ireland, *in* R.S. Arthurson, P. Gutteridge and S.C. Nolan, eds., Role of Tectonics in Devonian and Carboniferous Sedimentation in the British Isles: Spec. Publ. Yorkshire Geol. Soc., v. 6, p. 123-141.

Williams, E.A., 2000, Flexural cantilever models of extensional subsidence in the Munster Basin (SW Ireland) and Old Red Sandstone fluvial dispersal systems: Geological Society, London, Special Publications, v. 180, p. 239–268, doi: 10.1144/GSL.SP.2000.180.01.12.

Figures:

Fig. 1. Simplified geological map of the Munster Basin and the South Munster Basin in SW Ireland. The Munster Basin is defined by the Coomnacronia-Killarney-Mallow Fault Zone (CKMFZ) or alternatively by the Dingle Bay-Galtee Fault Zone (DB-GFZ) in the North. The Cork-Kenmare Fault Zone (CKFZ) indicates the rim to the South Munster Sub-Basin. An NNW directed compression indicates the Variscan Orogeny (modified from Geological Survey Ireland, GSI 2016; Sanderson 1984; Williams 2000; MacCarthy *et al.* 2002; Landes *et al.* 2003; MacCarthy 2007; Ennis *et al.* 2015).

Fig. 2. (a) Geological map with research localities, major lithologies of the South Munster Basin and mainly Variscan NE-SW striking fractures (modified from Geological Survey Ireland 2016). (b) Simplified profile of the Munster Basin sedimentary formations including the copper hosting transition zone at the top of the Castlehaven Formation (modified from Snodin 1972; MacCarthy 1990; Wen *et al.* 1996; MacCarthy *et al.* 2002; Pracht and Sleeman 2002; GSI 2016 and Spinks *et al.* 2016; horizontal extension not to scale).

Fig. 3. Geological map with research localities, modified after Geological Survey Ireland (2016), including satellite image and bathymetry data interpretation (Bing™ Satellite Maps 2016-2019; GSI Infomar 2017) and historical mineralization localities (GSI Jetstream 2019): West Cork peninsulas with outcropping Upper Devonian and Lower Carboniferous sediments. Large scale E-W faults and N-S faults with their relation to historic copper lodes and mineralized sediments. The rose diagrams show the mean orientation of the pre-Variscan extensional E-W and ENE-WSW striking faults.

Fig. 4. Baurearagh on Beara Peninsula: (a) Structural map with detailed drone maps of the research area showing pre-Variscan E-W and N-S faults and quartz veins, as well as compressional NE-SW striking folds and faults (satellite base map modified from ESRI, ArcGIS 2019). (b) 3-dimensional photogrammetry drone model shows the topography effect of the steep dipping E-W striking fault. (c) Stockwork quartz veining within the red sandstone; smaller image: quartz vein hydraulic breccia with red sandstone clasts and green chlorite rims. (d) Syn-compressional en echelon quartz veins within the cleaved sandstone. (e) + (f) Microphotographs of the Baurearagh mapping area: (e) Quartz vein (Qz) with folded specular hematite (Hem) with deformation twinning. (f) Quartz vein (Qz) with elongate blocky quartz crystals and stylolites seamed by a mixture of quartz (Qz) and goethite (Gth).

Fig. 5. The Caha Pass with the Turners Rock Tunnel on Beara Peninsula: (a) Structural map with detailed drone maps of the research area showing pre-Variscan E-W faults and quartz veins, as well as compressional WSW-ENE to E-W striking folds and NE-SW striking faults (satellite base map modified from ESRI, ArcGIS 2019). (b) Up to 30 cm wide pre-Variscan E-W striking quartz vein (V) with syn-compressional stylolites. The stylolites within the quartz vein are sub-parallel to the host rock (siltstone) cleavage (S_1).

Fig. 6. The historic mines of Gortavallig on Sheep's Head: (a) Structural map with detailed drone maps of the mining area showing early E-W faults and mineralized veins, as well as compressional NE-SW striking cleavage (S_1), folds and faults (satellite base map modified from ESRI, ArcGIS 2019). (b) Field image of NE-SW striking syncline with reverse fault and en echelon veining along the fold limbs. (c) Iron-stained quartz vein (V) cut off by bedding (S_0) parallel thrust. (d) – (k) Microphotographs of mineralization at Gortavallig Mining Area: (d) Cataclastic deformed arsenopyrite (Apy) within quartz (Qz) vein and minor, very small chalcopyrite (Ccp) within the arsenopyrite, (reflected light, ppl). (e) Massive pyrite (Py) with galena (Gn) and quartz (Qz) vein filling, (reflected light, ppl). (f) Quartz vein (Qz) with syngenetic pyrite (Py), chalcopyrite (Ccp) and tetrahedrite (Ttr), (reflected light, ppl). (g) Quartz vein (Qz) within sandstone (Sst) next to slate (Sl.). Both quartz vein and slate are mineralized with chalcopyrite (Ccp), (reflected and transmitted light, xpl). (h) Conglomerate with chalcopyritized (Ccp) clasts within siltstone (Sltst) matrix (Killeen North Mine). One of the chalcopyritized (Ccp) clasts shows oval to elongated fossilised plant cells with minor tetrahedrite (Ttr), (reflected light, ppl).

Fig. 7. The copper mines of Dhurode on the northern coast of Mizen Peninsula: (a) Structural map with detailed drone maps of the research area showing pre-Variscan E-W faults, compressional NE-SW striking cleavage (S_1), as well as WSW-ENE oriented folds and faults (satellite base map

modified from ESRI, ArcGIS 2019). (b) Aerial drone image of the coastal area at Dhurode showing NE-SW striking host rock cleavage (S_1) and WSW-ENE striking anticline rimmed by two reverse faults. (c) Thin section of oriented, mineralized quartz vein (near mining shafts, cut perpendicularly to vein strike V) showing elongate blocky quartz crystals with undulous extinction and partially recrystallized microfault (transmitted light, xpl). (d) Microphotograph of mineralized quartz vein (Dhurode tailings) shows euhedral arsenopyrite (Apy) with syngenetic chalcopyrite (Ccp) and tetrahedrite (Ttr).

Fig. 8. The Crookhaven Copper Mines on the southern coast of Mizen Peninsula: (a) Structural map with detailed drone maps of the research area showing pre-Variscan NE-SW striking faults, parallel compressional cleavage (S_1), and NE-SW striking folds (satellite base map modified from ESRI, ArcGIS 2019). (b) Splaying horsetail quartz veinlets with vein cleavage ($S_{1,vein}$) sub-parallel to the host rock cleavage (S_1). (c) Siltstone (Sltst) with folded, mineralized quartz (Qz) veins with chalcopyrite (Ccp). (d) Mineralized quartz vein within malachite (Mlc) stained siltstone: The microphotographs show (A) disseminated chalcopyrite (Ccp) within the siltstone (Sltst), as well as (B) massive chalcopyrite (Ccp) with goethite (Gth) alteration within the quartz (Qz) vein (reflected light, ppl). (e) Microphotograph of quartz (Qz) vein with bornite (Bn) next to a sandstone (Sst) (reflected light, ppl). The microfracture (red line) is rimmed by quartz (Qz) and goethite (Gth). The close-up image shows cataclastic bornite (Bn) with minor chalcopyrite (Ccp) and chalcocite (Cct) and covellite (Cv) alterations. (f) Quartz (Qz) vein with chalcopyrite (Ccp), chlorite (Chl), goethite (Gth) and stylolites (reflected ring light, ppl). (g) Fibrous quartz (Qz) vein with parallel siderite (Sd) and minor chalcopyrite (Ccp) (high resolution optical scan).

Fig. 9. The Ballycummisk Copper Mines near the southern coast of Mizen Peninsula: (a) Structural map with inferred structures (modified after Bing™ Satellite Maps 2016-2019, Google Maps 2016-2019, and historic mining

maps from GSI Jetstream 2019) showing E-W, SW-NE, and N-S striking faults. (b) Microphotograph of tailings sample with barite (Brt), chalcopyrite (Ccp) and deformed, specular hematite (Hem) (reflected light, ppl). (c) Microphotograph of quartz-barite vein (Qz, Brt) with syngenetic chalcopyrite (Ccp) and molybdenite (Mol), as well as goethite (Gth) alterations (ring light, ppl). (d) High-resolution scan of hand specimen of quartz (Qz) vein with syngenetic chalcopyrite (Ccp) and molybdenite (Mol), as well as molybdenite aggregations along stylolites (please see Supplemental material: Local Observations for larger figures). (e) Microphotograph of quartz (Qz) vein with disseminated molybdenite (Mol), molybdenite aggregations along stylolites and minor, specular hematite (Hem). (f) Greenish altered slate (Sl.) with folded and cleaved quartz vein (Qz) which is cross-cut by cleavage-parallel quartz-barite-hematite veins (Qz, Brt, Hem) with chalcopyrite (Ccp) and malachite (Mlc) mineralization.

Fig. 10. Examples of fluid inclusions assemblages (FIAs) within quartz veins (microphotographs): (a) Ballycummisk (pre-Variscan): Oval to angular shaped fluid inclusions with large vapour phase (mineralized vein with molybdenite, Mol). (b) Dhurode (pre-Variscan): Mineralized quartz vein with chalcopyrite (Ccp) and oval shaped fluid inclusions with small vapour phase. (c) Crookhaven: Elongated fluid inclusions within syn-Variscan quartz vein. (d) Gortavallig: Large angular to oval shaped fluid inclusions from syn-Variscan quartz vein. See Appendix 2 for further FIAs.

Fig. 11. Fluid inclusions measurements from the selected research areas in West Cork (Fig. 3): Plot of the salinity wt% $NaCl_{equiv}$ versus the homogenization temperatures T_h (°C). The different colours show the various locations, and the symbols indicate the individual fluid inclusion assemblages (FIA) within one sample (see App. 2 for details). The dotted ovals indicate the measured values from Allihies (Fig. 3, Lang *et al.* 2020). (a) Early extensional (pre-Variscan) vein samples. (b) Compressional (syn-Variscan) vein samples. Further details are available in Appendix 2.

Fig. 12. Block model of the South Munster Basin in West Cork (including adaptions after Williams 2000; Landes *et al.* 2003 and SRTM digital terrain model from Jarvis *et al.* 2008). (a) The basinal E-W faults follow the strike of the major Cork-Kenmare Fault in the North. The E-W faults form the fluid pathways for the mineralized quartz veins which can be associated with sediment hosted copper beds. (b) A reactivation of these E-W faults during the Variscan Compression and crustal shortening can remobilize basin related copper mineralization.

Tables:

Area (Large-Scale)	Pre-Variscan (extensional) Structures	Syn-Variscan (compressional) Structures
Beara Peninsula (Fig. 1. 2a and 3)	E-W striking faults and fault systems (negative topographic features - photolineaments on satellite imaging data, Bing™ Satellite Maps 2016-2019); weathered trenches of ca. 3 to 40 m width and up to 8.4 km length; the mean strike direction of the faults is 089° (N = 301); the faults form narrow elongate bays along the coastline; some faults are associated with large (up to several hundred metres) E-W striking quartz veins → historically mined copper lodes (Geological Survey Ireland Jetstream 2019; Fig. 3, e.g. Allihies and north coast of Beara Peninsula); N-S striking faults (up to 4.3 km length) are generally not associated with quartz veins	Kilometre-scale ENE-WSW to E-W striking compressional first order folds and several hundreds of meters second order folds (Geological Survey Ireland 2016); the Beara Peninsula is formed by a large anticline; ENE-WSW striking reverse faults (Geological Survey Ireland 2016); pre-Variscan N-S faults are folded by syn-Variscan ENE-WSW to E-W striking compressional folds and show stronger folding than pre-Variscan E-W faults (nearly perpendicular to Variscan stress)
Sheep's Head Peninsula (Fig. 1, 2a, and 3)	E-W faults with a max. length of 4.7 km and mean strike of 089 (N = 63); E-W faults are associated with historically mined, mineralized quartz veins (Fig. 3, e.g. Gortavallig and Killeen North); N-S to NNE-SSW striking faults have a maximum length of up to 5 kilometres and are not associated with quartz veins	Kilometre-scale ENE-WSW to SW-NE striking compressional first order folds and several hundreds of meters second order folds (Geological Survey Ireland 2016); Sheep's Head Peninsula is formed by an anticline (first order fold); SW-NE and ENE-WSW striking compressional reverse folds (Geological Survey Ireland 2016); folded N-S to NNE-SSW striking pre-Variscan folds
Mizen Peninsula (Fig. 1, 2a, and 3)	E-W striking faults in the north-eastern part of Mizen Peninsula with max. 4.3 km length and a mean strike of 090° (N = 98); ENE-WSW striking faults in the southern part of Mizen Peninsula with a maximum length of 7 km and a mean strike of 082° (N = 115); the ENE-WSW faults can be followed offshore (Geological Survey Ireland Infomar 2017); E-W and ENE-WSW striking faults are sometimes associated with historic copper lodes (Fig. 3, e.g. Dhurode Mine and Crookhaven Mines); N-S striking faults have a maximum length of 6.6 km and are generally not associated with mineralized quartz veins	Kilometre-scale ENE-WSW to SW-NE striking compressional first order folds and several hundreds of meters second order folds (Geological Survey Ireland 2016); Mizen Peninsula is formed by two anticlines and one syncline (first order fold); SW-NE striking compressional reverse folds (Geological Survey Ireland 2016); folded N-S striking pre-Variscan folds

Table 1. *Large-scale (Peninsulas) structural pre-Variscan and syn-Variscan features in SW Ireland.*

Location	Coordinates (GCS_WGS_1984)	Lithology	Pre-Variscan Structures	Syn-Variscan Structures	Mineralization	Microstructures
Baurearagh	51.781766 (°N) -9.650353 (°E)	Mica-rich, beige to reddish-brown sandstones (Caha Mountain Formation; Geological Survey Ireland, GSI 2016) with individual beds up to 1 m thickness	E-W to ENE-WSW striking fault, dipping 57° to south (Figs 4a + 4b); quartz veins up to 40 metres length and 1.5 m in width (mean strike: 085°, N = 457); hydrofractures with stockwork veining (Fig. 4c); host rock clasts in veins (Fig. 4c)	Host rock cleavage (S_1) NE-SW to ENE-WSW, nearly vertical dip (Fig. 4a); SW to NE striking folds (Figs 4a + 4b); en echelon quartz veins (Fig. 4d); reactivated normal faults (Fig. 4b); slickenlines on E-W striking extensional quartz veins indicate N-W directed compressional movement; stylolites in quartz veins as weak form of cleavage (4f); minor faulting of pre-Variscan quartz veins	Quartz with chlorite, minor specular hematite in pre-Variscan quartz veins (Fig. 4e)	Pre-Variscan veins: Elongate blocky quartz; hematite is folded – deformation twinning (Fig. 4e); stylolites with goethite alignment (Fig. 4f) Syn-Variscan veins: Elongate blocky to stretched elongate blocky quartz
Caha Pass	51.785218 (°N) -9.590671 (°E)	Purple siltstone with ripple marks to greenish grey to beige siltstone (Slaheny Sandstone Formation; GSI 2016)	E-W striking faults with associated quartz veins with a maximum length of 37 metres and a width of up to 1 m (mean strike 089°, N = 48, Fig. 5a); massive quartz with occasional vugs with euhedral quartz crystals; stockwork veining; brecciated host rock clasts	Host rock cleavage (S_1) E-W to NE-SW, steep dip (Fig. 5a); WSW-ENE striking folds faulted by NE-SW striking reverse fault (Fig. 5a); pre-Variscan veinlets are folded and cleaved; stylolites (weak cleavage) in quartz veins (V) (Fig. 5b)	Quartz with major chlorite, minor iron hydroxides, very little malachite	Quartz vein with chlorite crosscut by later quartz vein generation with elongate stretched quartz crystals (syn-Variscan); both generations show stylolites
Gortavallig and Killeen North	Gortavallig: 51.575887 (°N) -9.784587 (°E) Killeen North: 51.597905 (°N) -9.727637 (°E)	Cross-bedded beige sandstone to grey-beige sandstone and mica-rich siltstone to grey sandy slates (Toe Head Formation; GSI 2016)	E-W to ENE-WSW striking faults (Fig. 6a); mineralized and partly mineralized E-W trending (087°, N = 38) quartz veins up to 1.5 m width and over 35 m length; massive veins with occasional vugs of euhedral quartz crystals (up to 2 cm)	Host rock cleavage (S_1) with a general NE-SW strike and a steep to vertical dip (Fig. 6a); NE-SW striking folds (Fig. 6a + 6b); semi brittle shear zones with en echelon quartz veining along the fold limbs (Fig. 6b); faulting and complete cut off extensional veins (V), (Figs 6a + 6c) by reverse faults (Fig. 6b); minor folding and cleavage of pre-Variscan quartz veins (Fig. 6c)	Quartz with iron hydroxides (goethite, Fig. 6c), chalcopyrite, euhedral arsenopyrite (Fig. 6d), aggregates of pyrite (Fig. 6e), very little galena and tetrahedrite (Figs 6e + 6f)	Chalcopyrite occurs in quartz veins as well as disseminated in slates next to the veins (Fig. 6g); the euhedral arsenopyrite is cataclasticly deformed (Variscan compression, Fig. 6d); a sample from Killeen North (Fig. 3) shows a conglomerate with a chalcopyritized (permineralized in chalcopyrite) plant fossil (Fig. 6h)
Dhurode	51.516135 (°N) -9.757177 (°E)	Brownish red to grey, cross-bedded silty sandstone and sandy siltstone (Toe	E-W to WNW-ESE and ENE-WSW striking faults (Fig. 7a); E-W striking quartz veins (V) up to 30 cm wide	Host rock cleavage (S_1) has a NE-SW strike and a steep to nearly vertical dip (Fig. 7a); WSW-ENE striking folds; the limbs of the	Fibrous quartz veins with minor siderite, elongate blocky quartz (Fig. 7c) and quartz vugs with euhedral crystals, locally	Sample (Fig. 7c): E-W striking quartz vein with elongate blocky crystals (< 7 mm) with an NE-SW c-axis orientation, the crystals in the vein centre show a

		Head Formation, GSI 2016); grey to beige silty mudstone (Old Head Sandstone Formation; GSI 2016)		anticline are cut by WSW-ENE striking reverse faults forming a triangle zone (Fig. 7a + 7b); NW-SE striking and steep dipping quartz veins up to 10 cm in width	intensive iron hydroxide staining (altered sulfides); tailing material with predominant chalcopyrite and euhedral arsenopyrite (vein and sediment hosted), minor tetrahedrite (Fig. 7d)	sweeping (Trouw *et al.* 2009) undulous extinction, the crystals at the rim are mainly dominated by patchy undulous extinction, within the vein is an NNW-SSE striking micro-fault (Variscan deformation)
Crookhaven	51.469561 (°N) -9.711099 (°E)	Greenish-grey mica-rich sandstone to grey phyllitic slate and pale white to greenish-grey siltstone (Castlehaven Formation; GSI 2016), herringbone cross stratification	NE-SW striking extensional faults (Fig. 8a); parallel aligned quartz veins (NE-SW) up to 30 m long and up to 50 cm wide; several quartz veins together form lodes of over 400 m length (Fig. 8a); veins (V) have a steep to nearly vertical dip with a mean strike of 075° (N = 680); splaying horsetail veinlets indicate sinistral extensional movement (Fig. 8b)	Host rock cleavage (S_1) NE-SW striking, and steeply dipping; NE-SW striking series of tight folds with 20 to 30 m wavelengths (Fig. 8a); the interlimb angle and the wavelength of the folds increases to the south; minor to intensive folding and cleavage (S_1) formation of pre-Variscan quartz veins (Fig. 8c)	Quartz with aggregates of chlorite, chalcopyrite (vein and sediment hosted, Fig. 8d), siderite and barite, iron hydroxide (goethite) and malachite staining (Fig. 8d), small amounts of bornite, chalcocite and covellite (Fig. 8e)	Quartz vein with microfractures and cataclasticly fractured bornite (Fig. 8e); elongate blocky quartz with tectonic stylolites (Fig. 8f); fibrous quartz-siderite bands with deformation kinks of up to 90 degrees (crack-seal event, Fig. 8g)
Ballycummisk	51.533050 (°N) -9.476797 (°E)	Beige, silty sandstone (Castlehaven Formation and Toe Head Formation; GSI 2016)	Two ENE-WSW striking faults merge to one NE-SW oriented fault in the West (poor outcrop, blue dashed lines Fig. 9a; identification with historic mining maps from GSI Jetstream 2019 and Bing™ Satellite Maps 2016-2019 and Google Maps 2016-2019); NNW-SSE parallel striking faults (possibly pre-Variscan, Fig. 9a)	NE-SW striking fault crosscuts the pre-Variscan NE-SW striking structures (poor outcrop, possibly syn-Variscan, Fig. 9a; identification with historic mining maps from GSI Jetstream 2019 and Bing™ Satellite Maps 2016-2019 and Google Maps 2016-2019); reactivation of pre-Variscan faults; slightly folding of NNW-SSE faults	Recent tailings samples as well as historic molybdenite sample (BM.1964,R230) collected by Sir Arthur Russell in 1907 from the Ballycummisk Mine dumps directly located next to the collapsed mine shafts: Quartz veins with aggregates of chalcopyrite and tetrahedrite, white to red barite, specular hematite, chlorite encrustations, molybdenite aggregates and disseminated radial crystals (Figs 9b, 9c, 9d, 9e); molybdenite and chalcopyrite are syngenetically intergrown (Fig. 9c)	Recent tailings samples as well as historic molybdenite sample (BM.1964,R230) collected by Sir Arthur Russell in 1907 from the Ballycummisk Mine dumps directly located next to the collapsed mine shafts: Folded quartz-barite-hematite veins in pale yellow altered mudstone - partially deformed specular hematite (Fig. 9b); stylolites (weak cleavage) within quartz veins and molybdenite as residuum mineral along the stylolites (Fig. 9d + 9e); folded mineralized quartz vein (pre-deformation, Fig. 9f) crosscut by cleavage parallel barite-quartz-hematite-chalcopyrite vein (syn-/post-deformation)

Table 2. *Detailed geological features of selected localities in SW Ireland.*

Sample	*Sample wt (g)*	*Re (ppm)*	*±2σ*	^{187}Re *(ppm)*	*±2σ*	^{187}*Os (ppb)*	*±2σ*	*Model age (Ma)**	*±2σ*†	*±2σ*‡	*±2σ*§
BM.1964,R230	0.020	70.7	0.3	44.4	0.2	231.3	0.7	311.8	0.2	1.3	1.6
JL_BC_525	0.022	113.5	0.4	71.3	0.3	375.9	1.2	315.5	0.2	1.3	1.6

All data blank corrected (Re – 1.9 pg, Os – 0.8 pg with an $^{187}Os/^{188}Os$ of 0.201 ± 0.03)

**Model age calculated using the decay constant $^{187}Re = 1.666 \times 10^{-11}\ a^{-1}$ (Smoliar et al. 1996; Selby et al. 2007)*

†uncertainty including only mass spectrometry uncertainty

‡uncertainty including all sources of analytical uncertainty

§uncertainty including all sources of analytical uncertainty plus decay constant

Table 3. *Re-Os isotope data for the molybdenite samples BM.1964,R230 and JL_BC_525 (Fig. 9c) from Ballycummisk Mine (Fig. 3 + 9a; App. Table A1).*

Area (Large-Scale)	Pre-Variscan (extensional) Structures	Syn-Variscan (compressional) Structures
Beara Peninsula (Fig. 1. 2a and 3)	E-W striking faults and fault systems (negative topographic features - photolineaments on satellite imaging data, Bing™ Satellite Maps 2016-2019); weathered trenches of ca. 3 to 40 m width and up to 8.4 km length; the mean strike direction of the faults is 089° (N = 301); the faults form narrow elongate bays along the coastline; some faults are associated with large (up to several hundred metres) E-W striking quartz veins → historically mined copper lodes (Geological Survey Ireland Jetstream 2019; Fig. 3, e.g. Allihies and north coast of Beara Peninsula); N-S striking faults (up to 4.3 km length) are generally not associated with quartz veins	Kilometre-scale ENE-WSW to E-W striking compressional first order folds and several hundreds of meters second order folds (Geological Survey Ireland 2016); the Beara Peninsula is formed by a large anticline; ENE-WSW striking reverse faults (Geological Survey Ireland 2016); pre-Variscan N-S faults are folded by syn-Variscan ENE-WSW to E-W striking compressional folds and show stronger folding than pre-Variscan E-W faults (nearly perpendicular to Variscan stress)
Sheep's Head Peninsula (Fig. 1, 2a, and 3)	E-W faults with a max. length of 4.7 km and mean strike of 089 (N = 63); E-W faults are associated with historically mined, mineralized quartz veins (Fig. 3, e.g. Gortavallig and Killeen North); N-S to NNE-SSW striking faults have a maximum length of up to 5 kilometres and are not associated with quartz veins	Kilometre-scale ENE-WSW to SW-NE striking compressional first order folds and several hundreds of meters second order folds (Geological Survey Ireland 2016); Sheep's Head Peninsula is formed by an anticline (first order fold); SW-NE and ENE-WSW striking compressional reverse folds (Geological Survey Ireland 2016); folded N-S to NNE-SSW striking pre-Variscan folds
Mizen Peninsula (Fig. 1, 2a, and 3)	E-W striking faults in the north-eastern part of Mizen Peninsula with max. 4.3 km length and a mean strike of 090° (N = 98); ENE-WSW striking faults in the southern part of Mizen Peninsula with a maximum length of 7 km and a mean strike of 082° (N = 115); the ENE-WSW faults can be followed offshore (Geological Survey Ireland Infomar 2017); E-W and ENE-WSW striking faults are sometimes associated with historic copper lodes (Fig. 3, e.g. Dhurode Mine and Crookhaven Mines); N-S striking faults have a maximum length of 6.6 km and are generally not associated with mineralized quartz veins	Kilometre-scale ENE-WSW to SW-NE striking compressional first order folds and several hundreds of meters second order folds (Geological Survey Ireland 2016); Mizen Peninsula is formed by two anticlines and one syncline (first order fold); SW-NE striking compressional reverse folds (Geological Survey Ireland 2016); folded N-S striking pre-Variscan folds

Table 1. *Large-scale (Peninsulas) structural pre-Variscan and syn-Variscan features in SW Ireland.*

Location	Coordinates (GCS_WGS_1984)	Lithology	Pre-Variscan Structures	Syn-Variscan Structures	Mineralization	Microstructures
Baurearagh	51.781766 (°N) -9.650353 (°E)	Mica-rich, beige to reddish-brown sandstones (Caha Mountain Formation; Geological Survey Ireland, GSI 2016) with individual beds up to 1 m thickness	E-W to ENE-WSW striking fault, dipping 57° to south (Figs 4a + 4b); quartz veins up to 40 metres length and 1.5 m in width (mean strike: 085°, N = 457); hydrofractures with stockwork veining (Fig. 4c); host rock clasts in veins (Fig. 4c)	Host rock cleavage (S_1) NE-SW to ENE-WSW, nearly vertical dip (Fig. 4a); SW to NE striking folds (Figs 4a + 4b); en echelon quartz veins (Fig. 4d); reactivated normal faults (Fig. 4b); slickenlines on E-W striking extensional quartz veins indicate N-W directed compressional movement; stylolites in quartz veins as weak form of cleavage (4f); minor faulting of pre-Variscan quartz veins	Quartz with chlorite, minor specular hematite in pre-Variscan quartz veins (Fig. 4e)	Pre-Variscan veins: Elongate blocky quartz; hematite is folded – deformation twinning (Fig. 4e); stylolites with goethite alignment (Fig. 4f) Syn-Variscan veins: Elongate blocky to stretched elongate blocky quartz
Caha Pass	51.785218 (°N) -9.590671 (°E)	Purple siltstone with ripple marks to greenish grey to beige siltstone (Slaheny Sandstone Formation; GSI 2016)	E-W striking faults with associated quartz veins with a maximum length of 37 metres and a width of up to 1 m (mean strike 089°, N = 48, Fig. 5a); massive quartz with occasional vugs with euhedral quartz crystals; stockwork veining; brecciated host rock clasts	Host rock cleavage (S_1) E-W to NE-SW, steep dip (Fig. 5a); WSW-ENE striking folds faulted by NE-SW striking reverse fault (Fig. 5a); pre-Variscan veinlets are folded and cleaved; stylolites (weak cleavage) in quartz veins (V) (Fig. 5b)	Quartz with major chlorite, minor iron hydroxides, very little malachite	Quartz vein with chlorite crosscut by later quartz vein generation with elongate stretched quartz crystals (syn-Variscan); both generations show stylolites
Gortavallig and Killeen North	Gortavallig: 51.575887 (°N) -9.784587 (°E) Killeen North: 51.597905 (°N) -9.727637 (°E)	Cross-bedded beige sandstone to grey-beige sandstone and mica-rich siltstone to grey sandy slates (Toe Head Formation; GSI 2016)	E-W to ENE-WSW striking faults (Fig. 6a); mineralized and partly mineralized E-W trending (087°, N = 38) quartz veins up to 1.5 m width and over 35 m length; massive veins with occasional vugs of euhedral quartz crystals (up to 2 cm)	Host rock cleavage (S_1) with a general NE-SW strike and a steep to vertical dip (Fig. 6a); NE-SW striking folds (Fig. 6a + 6b); semi brittle shear zones with en echelon quartz veining along the fold limbs (Fig. 6b); faulting and complete cut off extensional veins (V), (Figs 6a + 6c) by reverse faults (Fig. 6b); minor folding and cleavage of pre-Variscan quartz veins (Fig. 6c)	Quartz with iron hydroxides (goethite, Fig. 6c), chalcopyrite, euhedral arsenopyrite (Fig. 6d), aggregates of pyrite (Fig. 6e), very little galena and tetrahedrite (Figs 6e + 6f)	Chalcopyrite occurs in quartz veins as well as disseminated in slates next to the veins (Fig. 6g); the euhedral arsenopyrite is cataclasticly deformed (Variscan compression, Fig. 6d); a sample from Killeen North (Fig. 3) shows a conglomerate with a chalcopyritized (permineralized in chalcopyrite) plant fossil (Fig. 6h)
Dhurode	51.516135 (°N) -9.757177 (°E)	Brownish red to grey, cross-bedded silty sandstone and sandy siltstone (Toe Head Formation, GSI 2016); grey to beige silty mudstone (Old Head Sandstone	E-W to WNW-ESE and ENE-WSW striking faults (Fig. 7a); E-W striking quartz veins (V) up to 30 cm wide	Host rock cleavage (S_1) has a NE-SW strike and a steep to nearly vertical dip (Fig. 7a); WSW-ENE striking folds; the limbs of the anticline are cut by WSW-ENE striking reverse faults forming a triangle zone (Fig. 7a + 7b); NW-SE striking and steep dipping quartz veins up to 10 cm in width	Fibrous quartz veins with minor siderite, elongate blocky quartz (Fig. 7c) and quartz vugs with euhedral crystals, locally intensive iron hydroxide staining (altered sulfides); tailing material with predominant chalcopyrite and euhedral arsenopyrite (vein	Sample (Fig. 7c): E-W striking quartz vein with elongate blocky crystals (< 7 mm) with an NE-SW c-axis orientation, the crystals in the vein centre show a sweeping (Trouw *et al.* 2009) undulous extinction, the crystals at the rim are mainly dominated by patchy undulous extinction, within the vein is an NNW-SSE

		Formation; GSI 2016)			and sediment hosted), minor tetrahedrite (Fig. 7d)	striking micro-fault (Variscan deformation)
Crookhaven	51.469561 (°N) -9.711099 (°E)	Greenish-grey mica-rich sandstone to grey phyllitic slate and pale white to greenish-grey siltstone (Castlehaven Formation; GSI 2016), herringbone cross stratification	NE-SW striking extensional faults (Fig. 8a); parallel aligned quartz veins (NE-SW) up to 30 m long and up to 50 cm wide; several quartz veins together form lodes of over 400 m length (Fig. 8a); veins (V) have a steep to nearly vertical dip with a mean strike of 075° (N = 680); splaying horsetail veinlets indicate sinistral extensional movement (Fig. 8b)	Host rock cleavage (S_1) NE-SW striking, and steeply dipping; NE-SW striking series of tight folds with 20 to 30 m wavelengths (Fig. 8a); the interlimb angle and the wavelength of the folds increases to the south; minor to intensive folding and cleavage (S_1) formation of pre-Variscan quartz veins (Fig. 8c)	Quartz with aggregates of chlorite, chalcopyrite (vein and sediment hosted, Fig. 8d), siderite and barite, iron hydroxide (goethite) and malachite staining (Fig. 8d), small amounts of bornite, chalcocite and covellite (Fig. 8e)	Quartz vein with microfractures and cataclasticly fractured bornite (Fig. 8e); elongate blocky quartz with tectonic stylolites (Fig. 8f); fibrous quartz-siderite bands with deformation kinks of up to 90 degrees (crack-seal event, Fig. 8g)
Ballycummisk	51.533050 (°N) -9.476797 (°E)	Beige, silty sandstone (Castlehaven Formation and Toe Head Formation; GSI 2016)	Two ENE-WSW striking faults merge to one NE-SW oriented fault in the West (poor outcrop, blue dashed lines Fig. 9a; identification with historic mining maps from GSI Jetstream 2019 and Bing™ Satellite Maps 2016-2019 and Google Maps 2016-2019); NNW-SSE parallel striking faults (possibly pre-Variscan, Fig. 9a)	NE-SW striking fault crosscuts the pre-Variscan NE-SW striking structures (poor outcrop, possibly syn-Variscan, Fig. 9a; identification with historic mining maps from GSI Jetstream 2019 and Bing™ Satellite Maps 2016-2019 and Google Maps 2016-2019); reactivation of pre-Variscan faults; slightly folding of NNW-SSE faults	Recent tailings samples as well as historic molybdenite sample (BM.1964,R230) collected by Sir Arthur Russell in 1907 from the Ballycummisk Mine dumps directly located next to the collapsed mine shafts: Quartz veins with aggregates of chalcopyrite and tetrahedrite, white to red barite, specular hematite, chlorite encrustations, molybdenite aggregates and disseminated radial crystals (Figs 9b, 9c, 9d, 9e); molybdenite and chalcopyrite are syngenetically intergrown (Fig. 9c)	Recent tailings samples as well as historic molybdenite sample (BM.1964,R230) collected by Sir Arthur Russell in 1907 from the Ballycummisk Mine dumps directly located next to the collapsed mine shafts: Folded quartz-barite-hematite veins in pale yellow altered mudstone - partially deformed specular hematite (Fig. 9b); stylolites (weak cleavage) within quartz veins and molybdenite as residuum mineral along the stylolites (Fig. 9d + 9e); folded mineralized quartz vein (pre-deformation, Fig. 9f) crosscut by cleavage parallel barite-quartz-hematite-chalcopyrite vein (syn-/post-deformation)

Table 2. *Detailed geological features of selected localities in SW Ireland.*

Sample	*Sample wt (g)*	*Re (ppm)*	*±2σ*	^{187}Re *(ppm)*	*±2σ*	^{187}*Os (ppb)*	*±2σ*	*Model age (Ma)**	*±2σ*†	*±2σ*‡	*±2σ*§
BM.1964,R230	0.020	70.7	0.3	44.4	0.2	231.3	0.7	311.8	0.2	1.3	1.6
JL_BC_525	0.022	113.5	0.4	71.3	0.3	375.9	1.2	315.5	0.2	1.3	1.6

All data blank corrected (Re – 1.9 pg, Os – 0.8 pg with an ^{187}Os/^{188}Os of 0.201 ± 0.03)

**Model age calculated using the decay constant ^{187}Re = 1.666 × 10^{-11} a^{-1} (Smoliar et al. 1996; Selby et al. 2007)*

†uncertainty including only mass spectrometry uncertainty

‡uncertainty including all sources of analytical uncertainty

§uncertainty including all sources of analytical uncertainty plus decay constant

Table 3. *Re-Os isotope data for the molybdenite samples BM.1964,R230 and JL_BC_525 (Fig. 9c) from Ballycummisk Mine (Fig. 3 + 9a; App. Table A1).*

figure

Click here to access/download;figure;Fig_1_Geology_Overview_Munster_Basin_2025.pdf

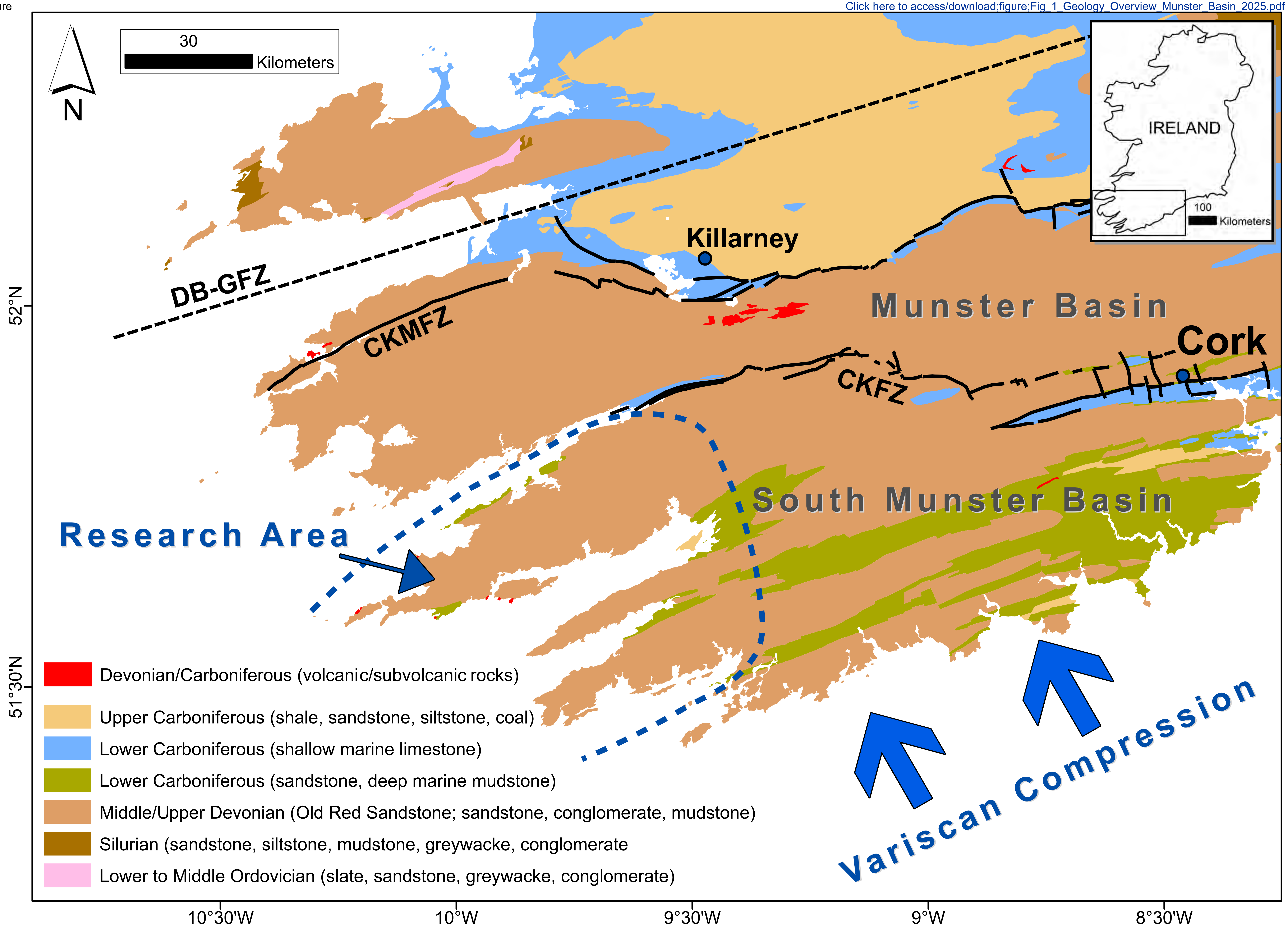

figure

Click here to access/download;figure;Fig_2_West_Cork_Sediments

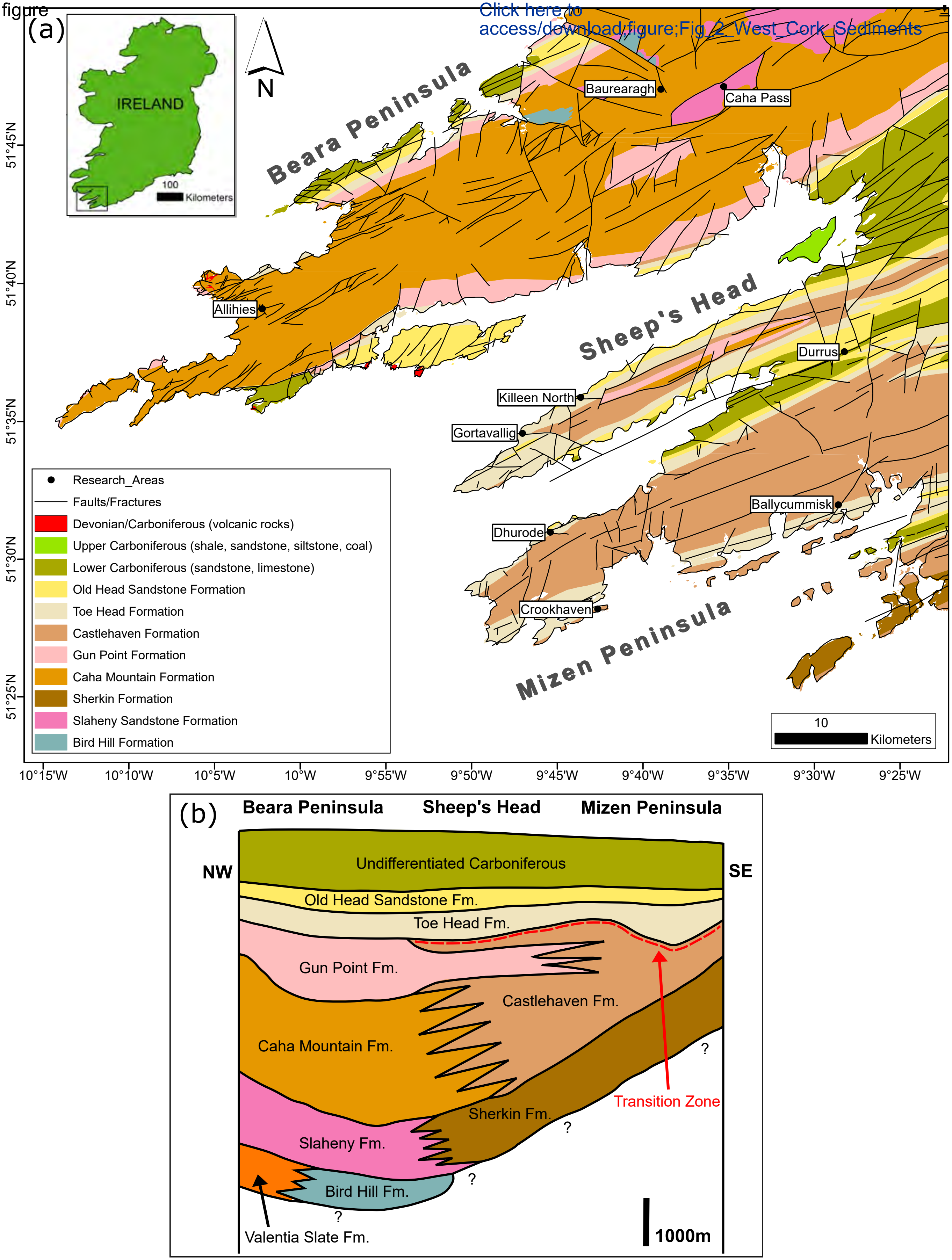

figure

Click here to access/download;figure;Fig_3_E-W_Faults_Cork_Structural_Overview_2025.pdf

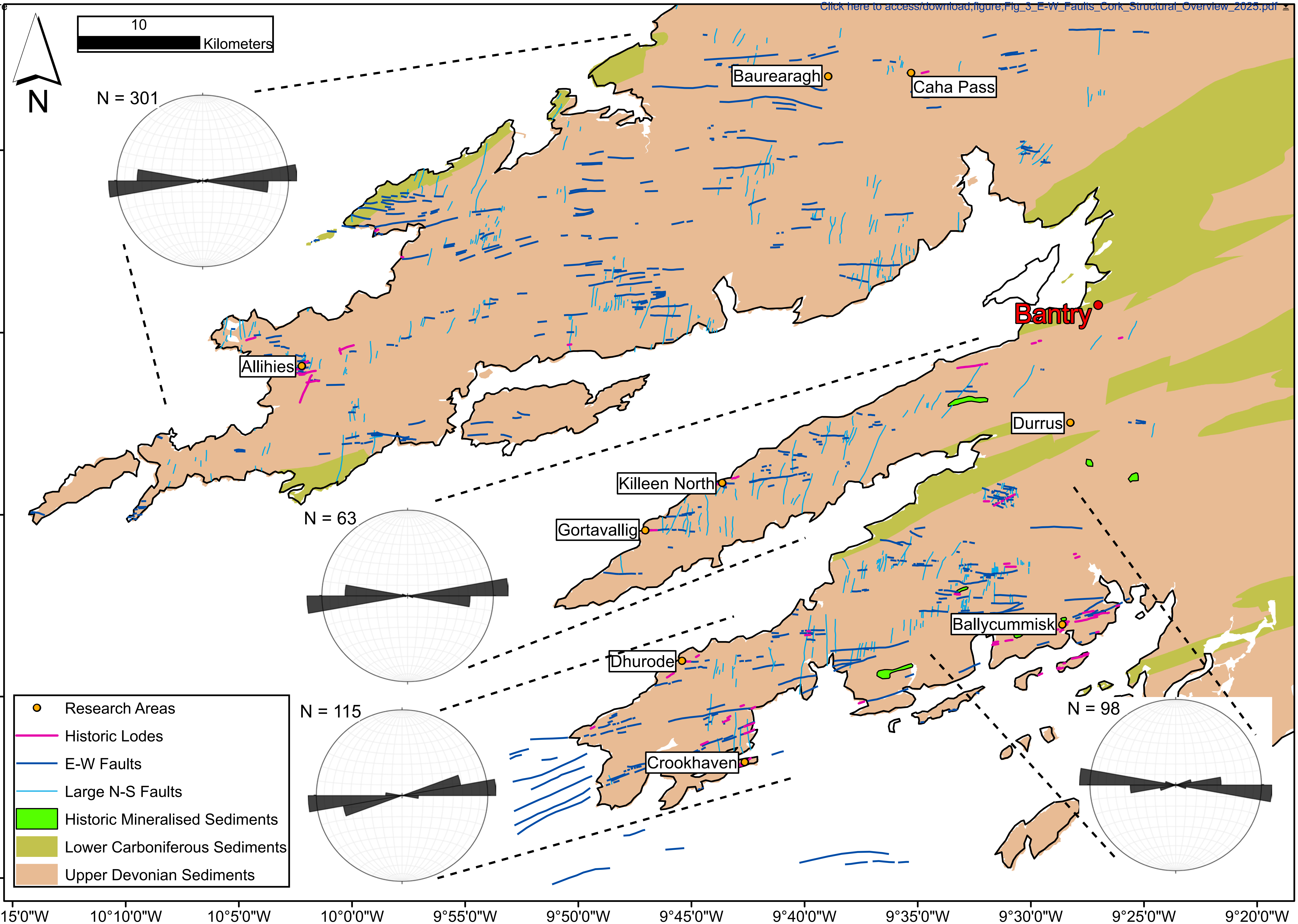

figure

Click here to access/download;figure;Fig_4_Location_Baurearagh_

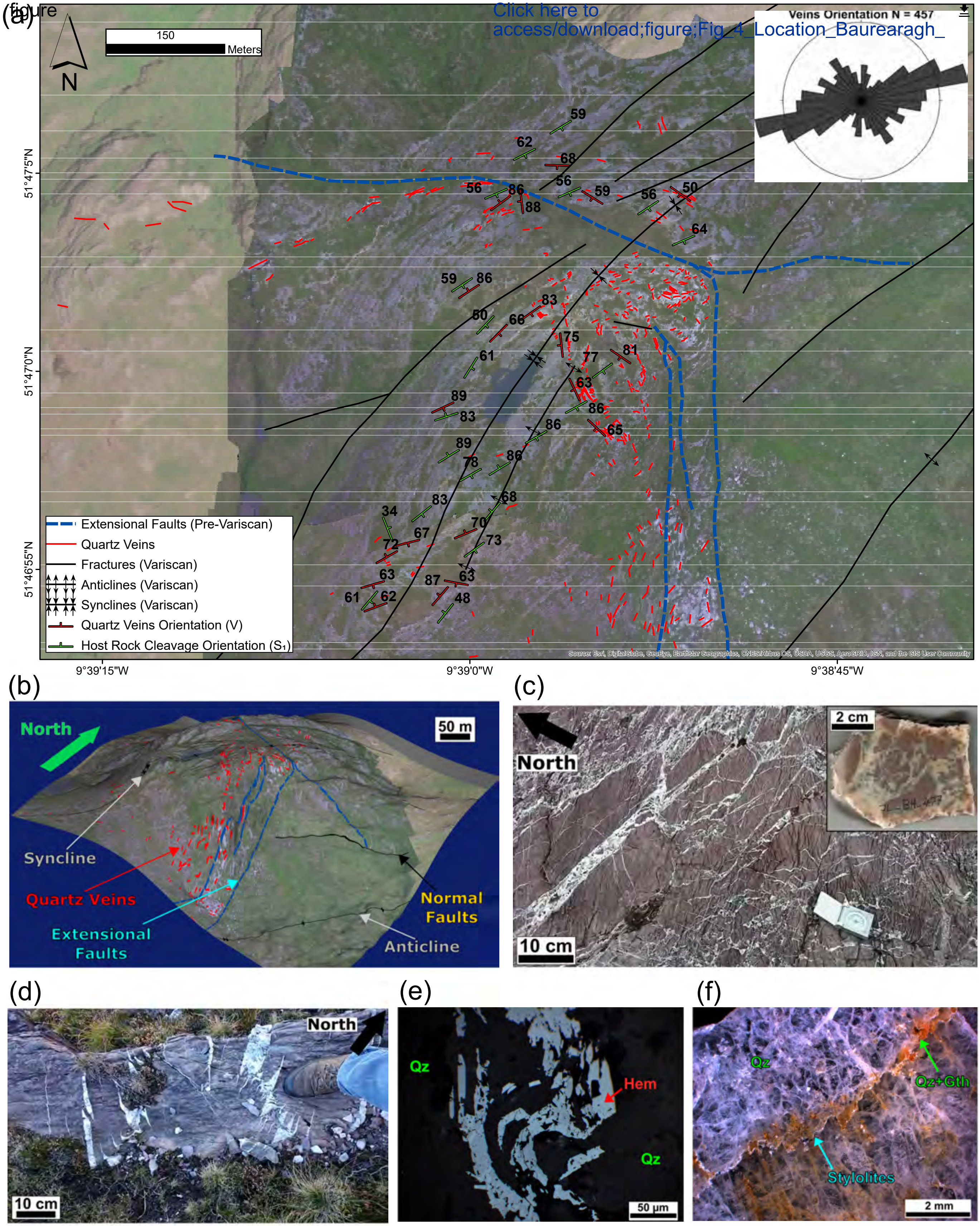

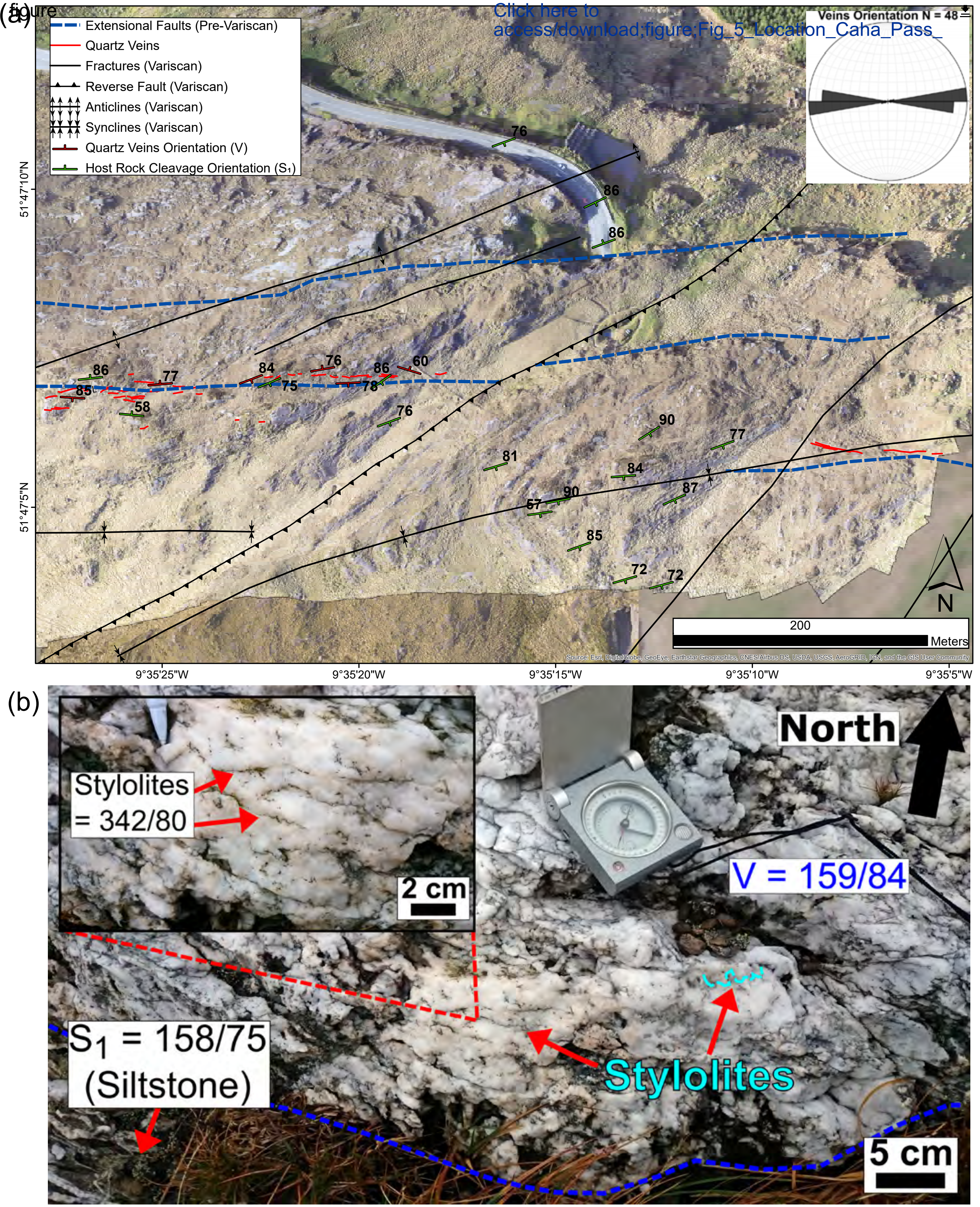
(a)
Extensional Faults (Pre-Variscan)
Quartz Veins
Fractures (Variscan)
Reverse Fault (Variscan)
Anticlines (Variscan)
Synclines (Variscan)
Quartz Veins Orientation (V)
Host Rock Cleavage Orientation (S₁)
Veins Orientation N = 48
51°47'10"N
51°47'5"N
9°35'25"W
9°35'20"W
9°35'15"W
9°35'10"W
9°35'5"W
N
200
Meters
(b)
Stylolites = 342/80
2 cm
North
V = 159/84
S1 = 158/75 (Siltstone)
Stylolites
5 cm

figure

Click here to access/download;figure;Fig_6_plateA_Location_Gortav

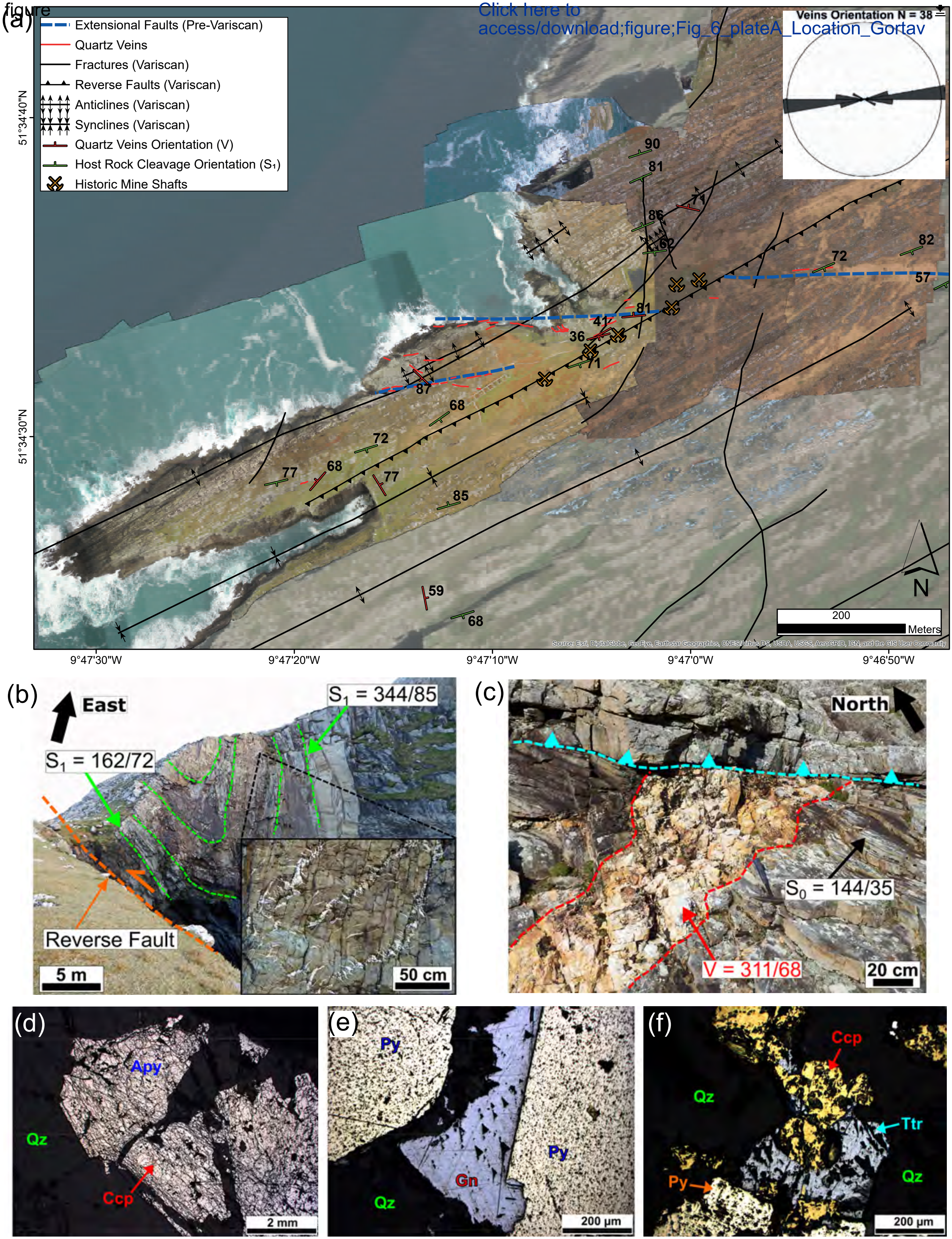

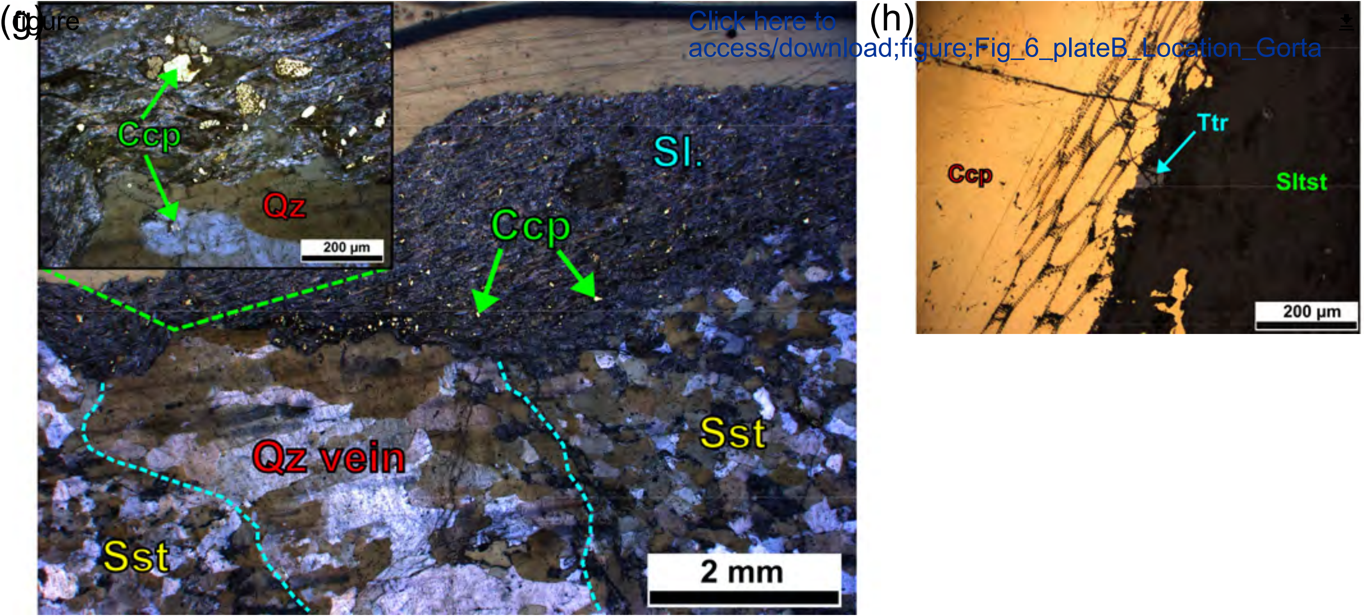
(g)
Ccp
Qz
200 µm
Sl.
Ccp
Sst
Qz vein
Sst
2 mm
(h)
Ttr
Ccp
Sltst
200 µm

figure

Click here to access/download;figure;Fig_7_Location_Dhurode_202

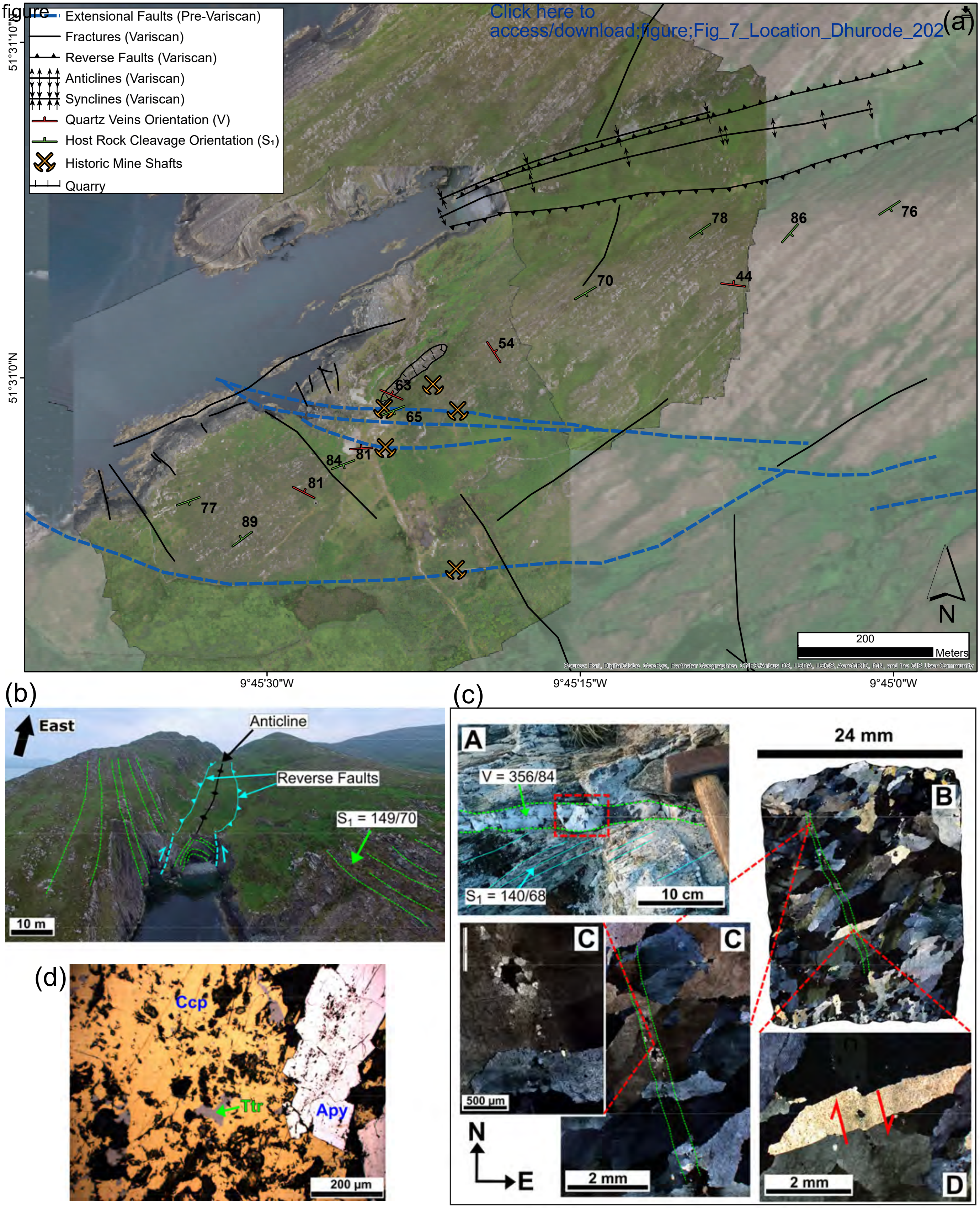

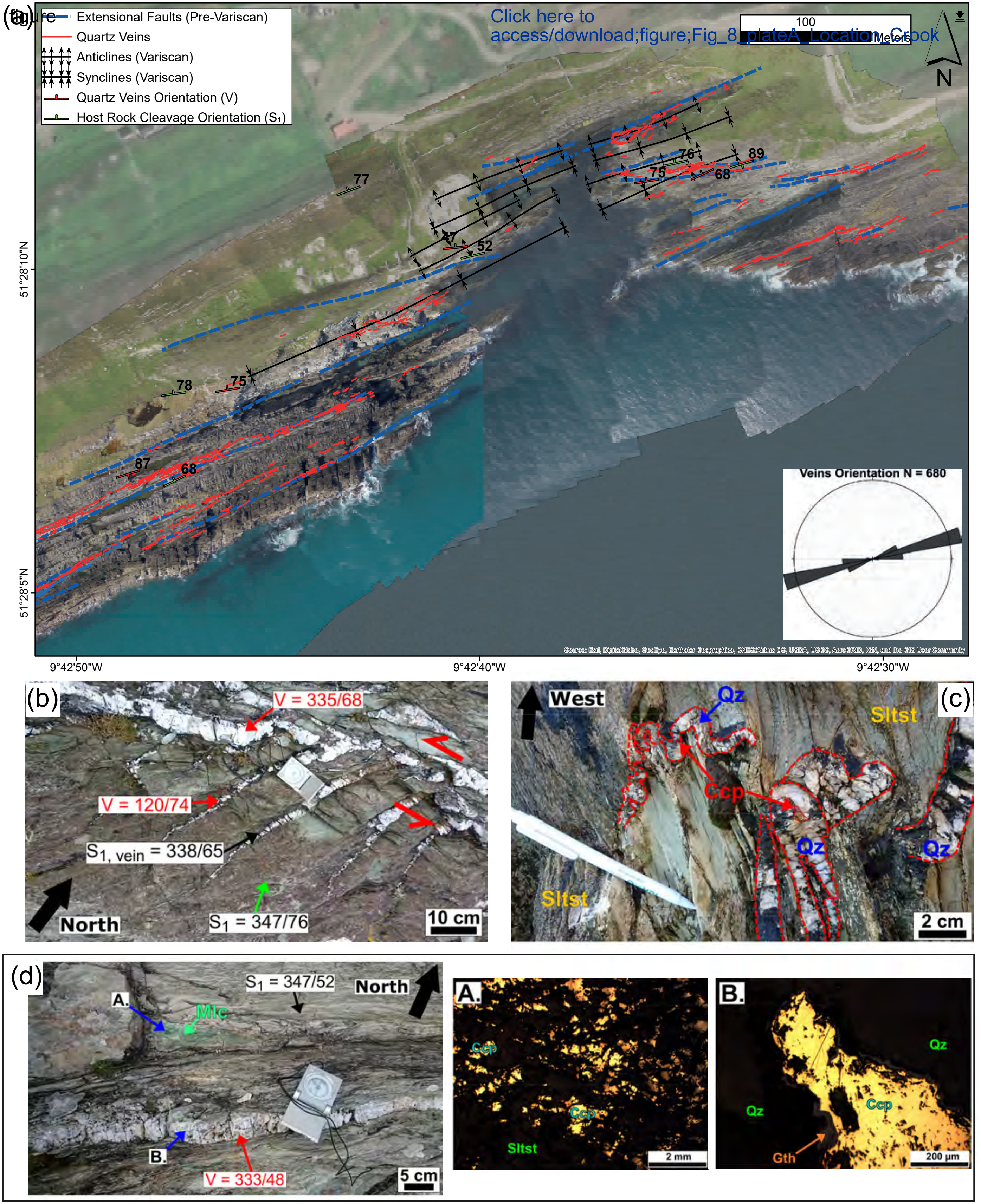
(a)
Extensional Faults (Pre-Variscan)
Quartz Veins
Anticlines (Variscan)
Synclines (Variscan)
Quartz Veins Orientation (V)
Host Rock Cleavage Orientation (S₁)
100
Meters
N
77
47
52
76
75
68
89
78
75
87
68
Veins Orientation N = 680
51°28'10"N
51°28'5"N
9°42'50"W
9°42'40"W
9°42'30"W
Source: Esri, DigitalGlobe, GeoEye, Earthstar Geographics, CNES/Airbus DS, USDA, USGS, AeroGRID, IGN, and the GIS User Community
(b)
V = 335/68
V = 120/74
S1, vein = 338/65
S1 = 347/76
North
10 cm
(c)
West
Qz
Sltst
Ccp
Qz
Qz
Sltst
2 cm
(d)
S1 = 347/52
North
A.
Mlc
B.
V = 333/48
5 cm
A.
Ccp
Ccp
Sltst
2 mm
B.
Qz
Qz
Ccp
Gth
200 μm

figure

Click here to access/download;figure;Fig_8_plateB_Location_Crook

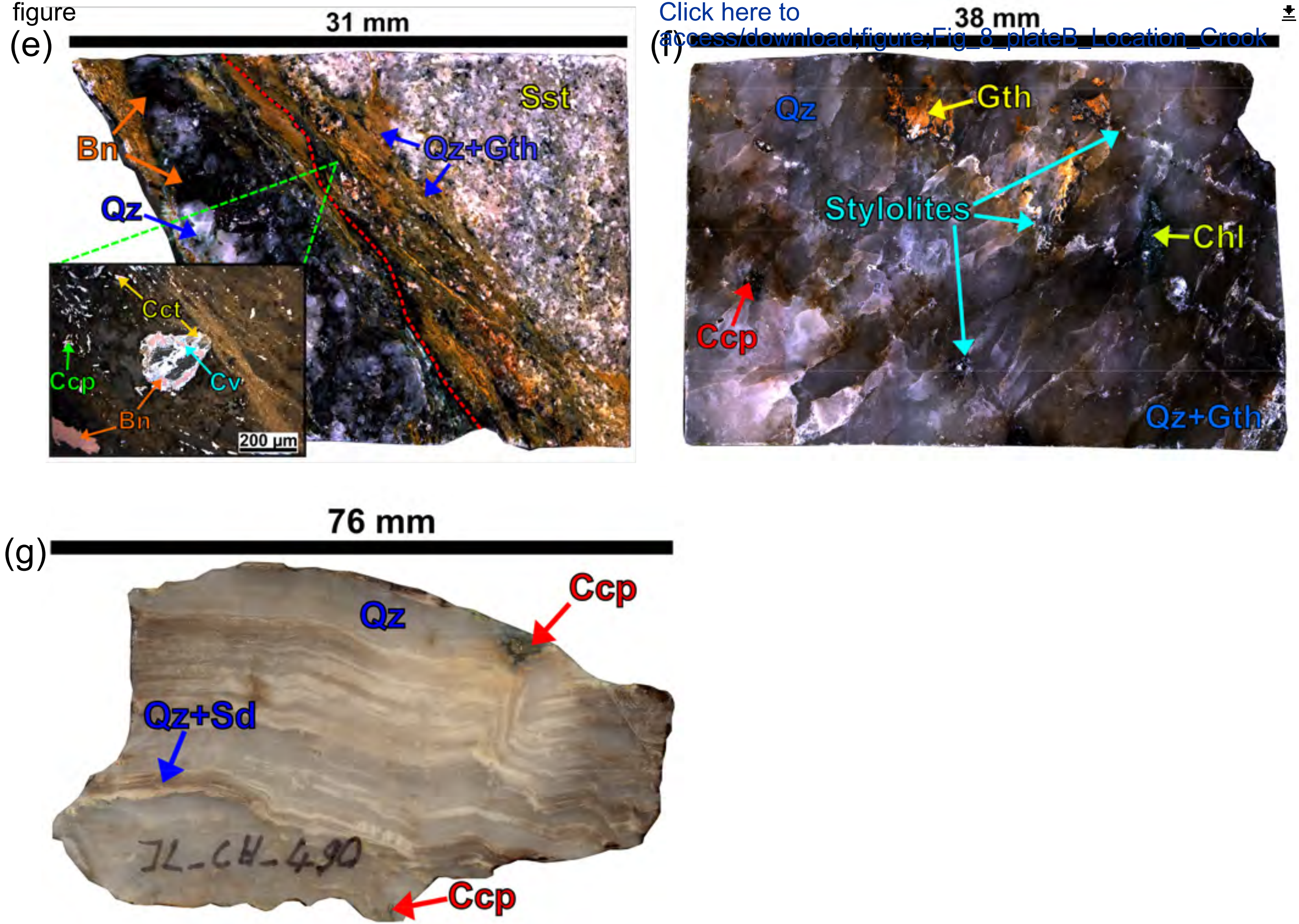

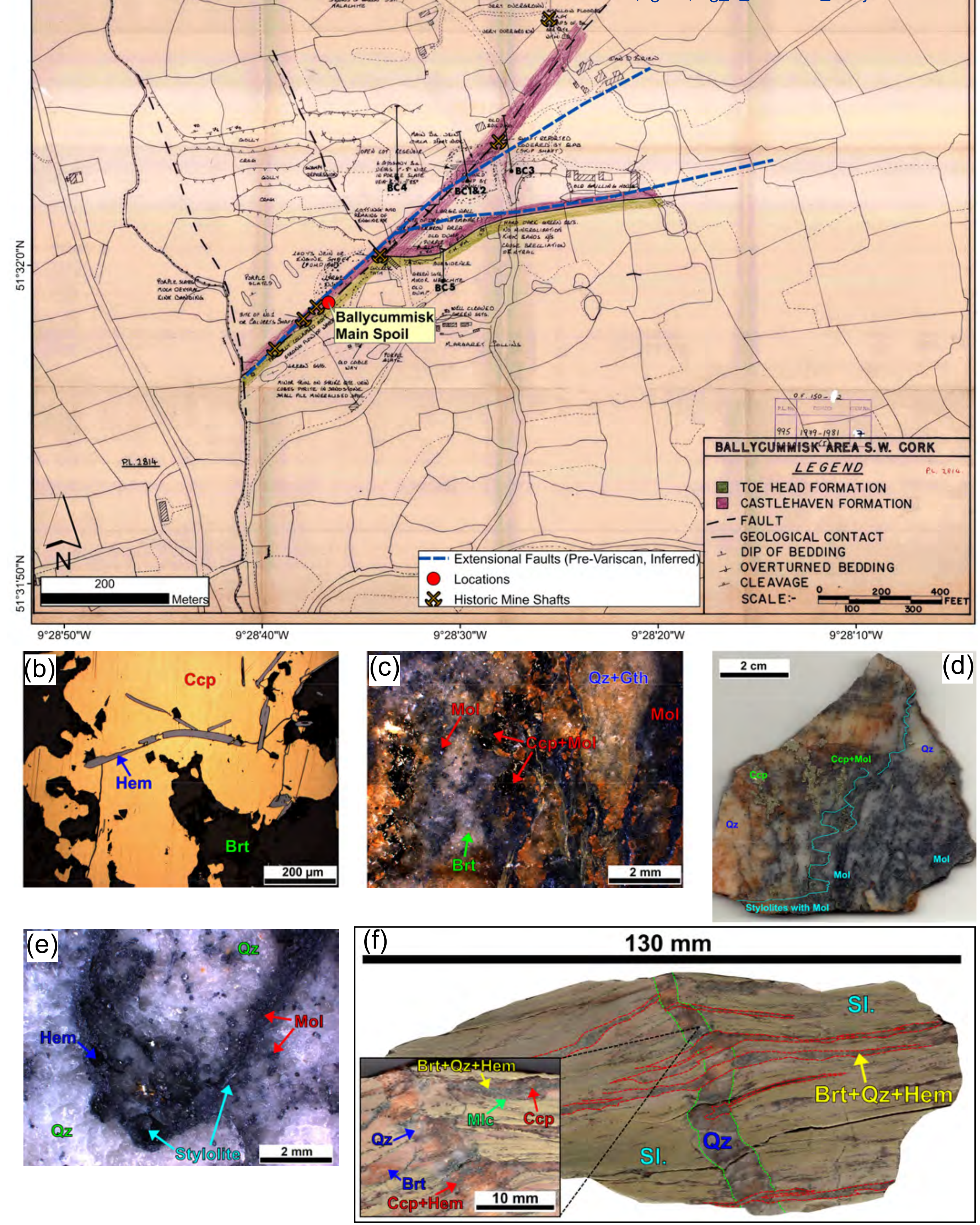
(a)
BC4
BC1&2
BC3
BC5
Ballycummisk Main Spoil
N
200
Meters
Extensional Faults (Pre-Variscan, Inferred)
Locations
Historic Mine Shafts
BALLYCUMMISK AREA S.W. CORK
LEGEND
TOE HEAD FORMATION
CASTLEHAVEN FORMATION
FAULT
GEOLOGICAL CONTACT
DIP OF BEDDING
OVERTURNED BEDDING
CLEAVAGE
SCALE:-
0
100
200
300
400
FEET
P.L. 2814
51°32'0"N
51°31'50"N
9°28'50"W
9°28'40"W
9°28'30"W
9°28'20"W
9°28'10"W
(b)
Ccp
Hem
Brt
200 µm
(c)
Qz+Gth
Mol
Ccp+Mol
Brt
2 mm
(d)
2 cm
Ccp
Ccp+Mol
Qz
Mol
Stylolites with Mol
(e)
Qz
Mol
Hem
Stylolite
2 mm
(f)
130 mm
Sl.
Brt+Qz+Hem
Mlc
Ccp
Qz
Brt
Ccp+Hem
10 mm

figure

Click here to access/download;figure;Fig_10_Fluid_Inclusions_Micr

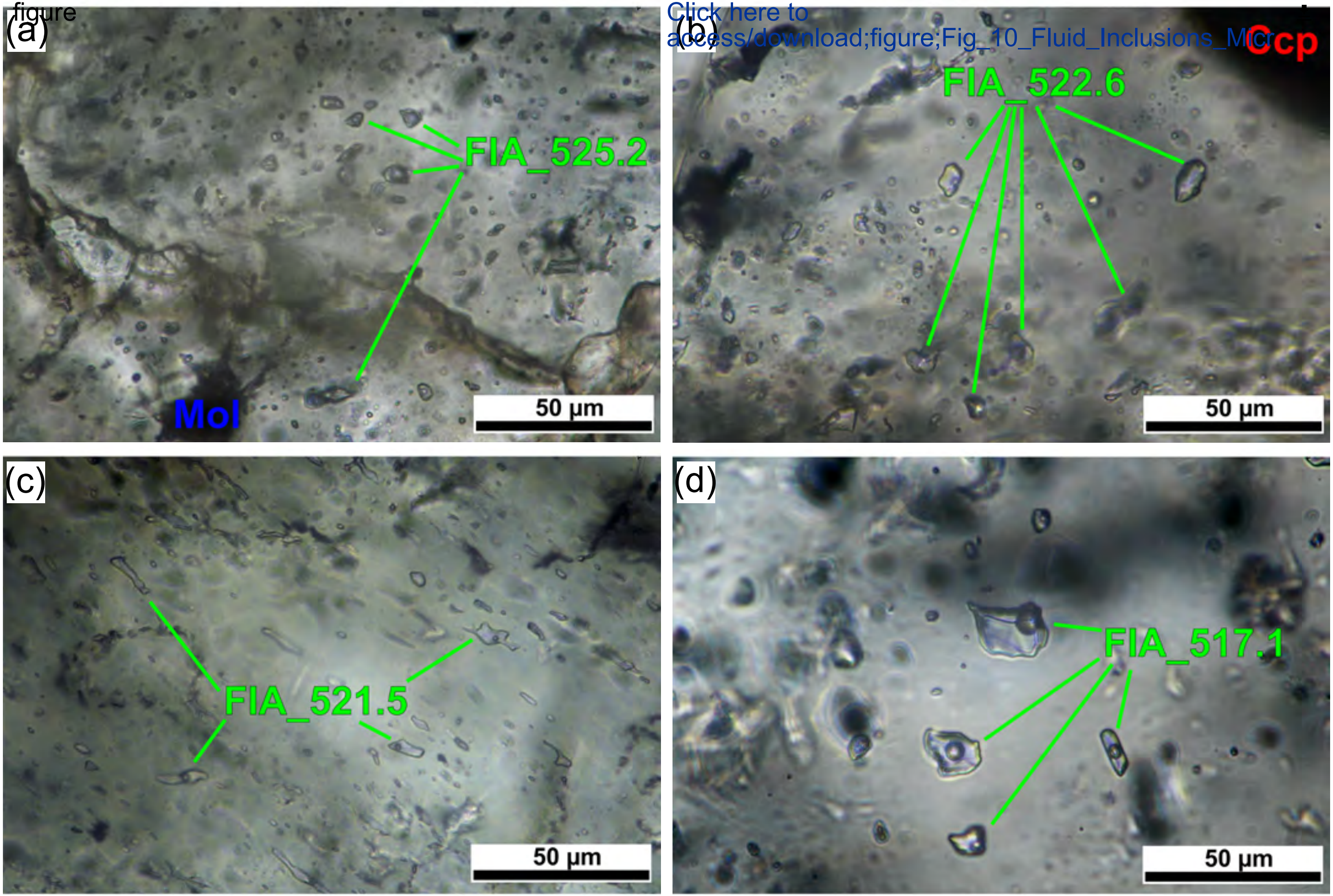

figure	Click here to access/download;figure;Fig_11_Fluid_Inclusions_Res

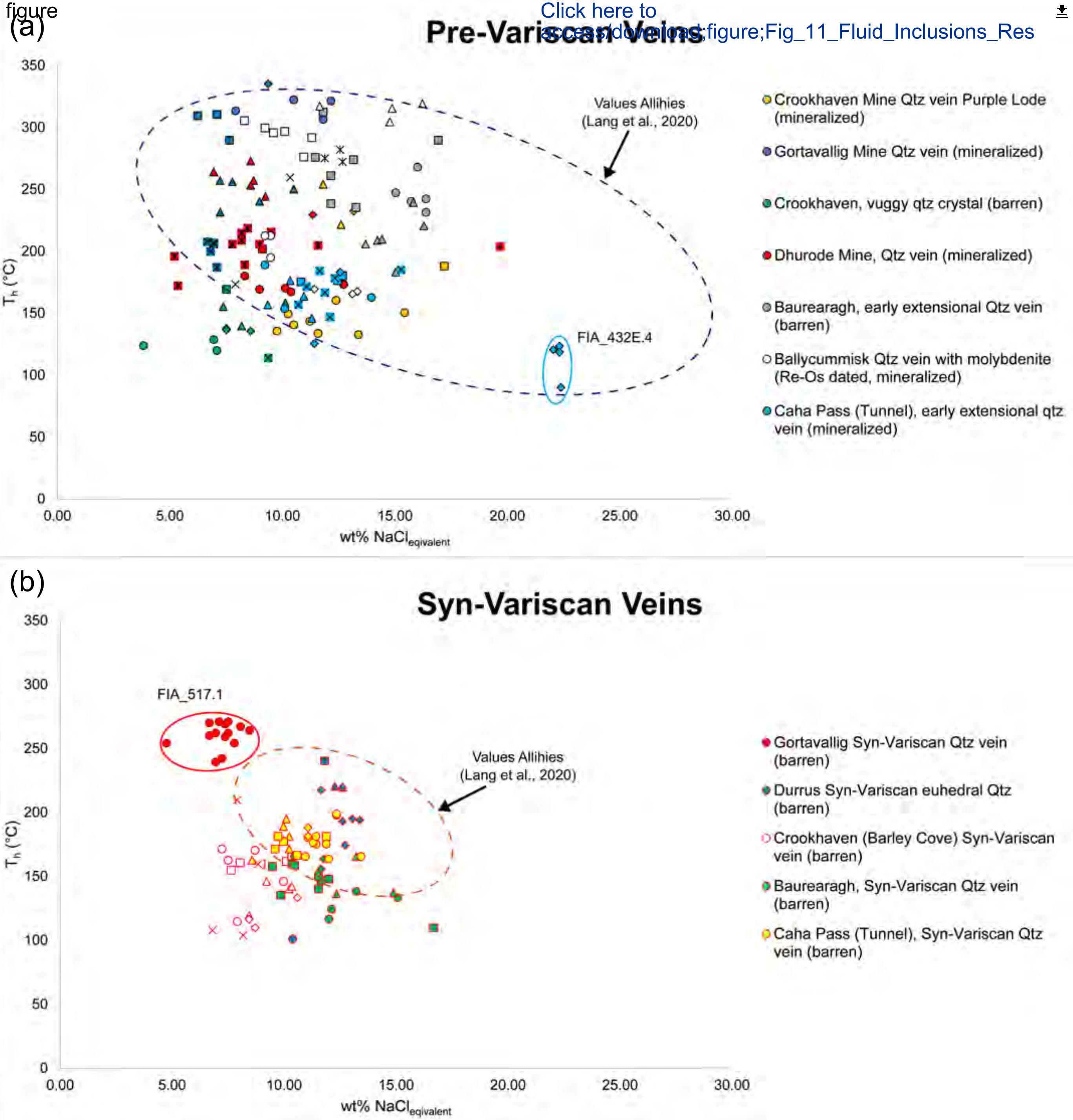

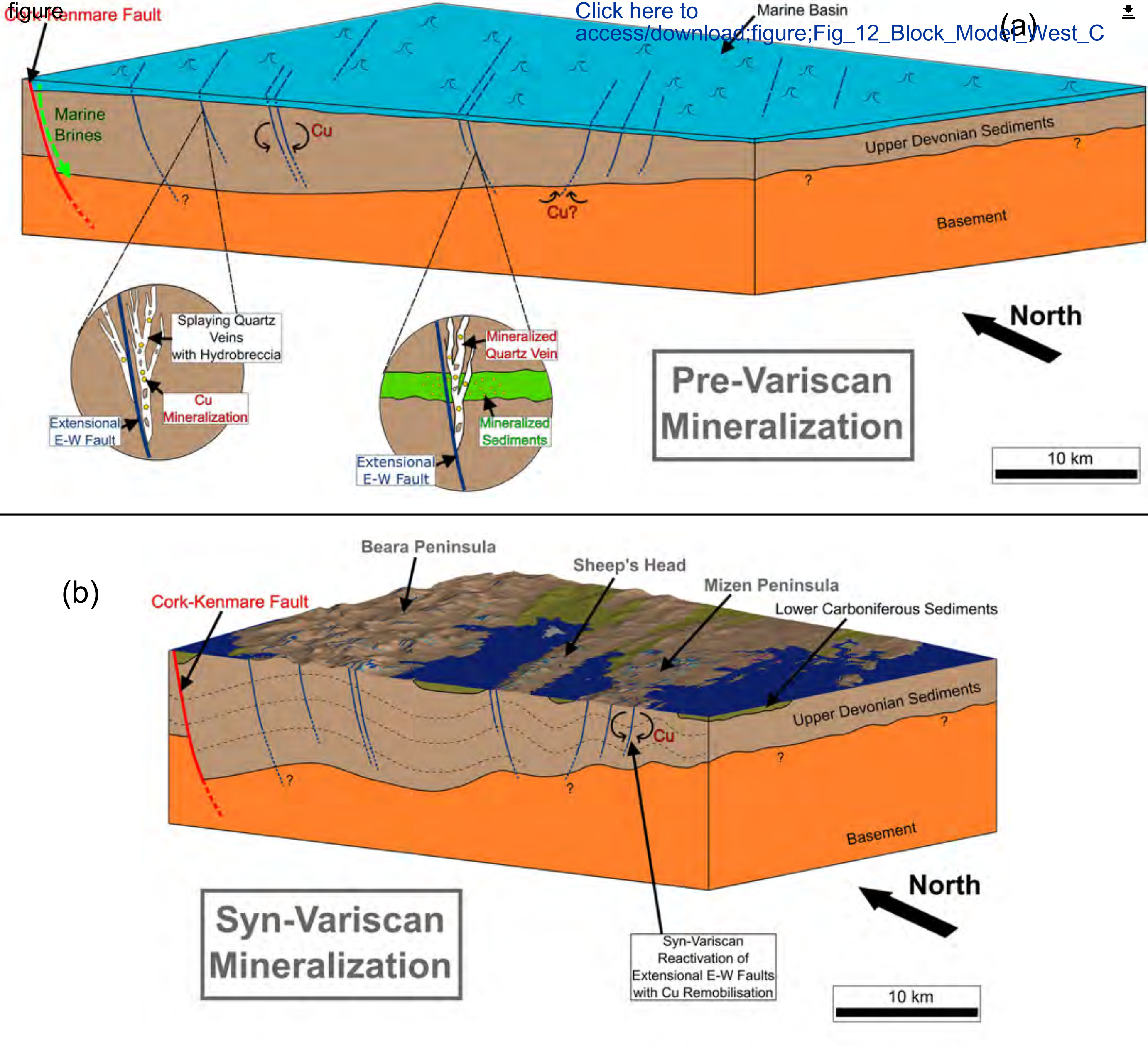
(a)
Cork-Kenmare Fault
Marine Basin
Marine Brines
Cu
Cu?
Upper Devonian Sediments
Basement
?
Splaying Quartz Veins with Hydrobreccia
Cu Mineralization
Extensional E-W Fault
Mineralized Quartz Vein
Mineralized Sediments
Extensional E-W Fault
North
Pre-Variscan Mineralization
10 km
(b)
Beara Peninsula
Sheep's Head
Mizen Peninsula
Lower Carboniferous Sediments
Cork-Kenmare Fault
Upper Devonian Sediments
Cu
Basement
North
Syn-Variscan Mineralization
Syn-Variscan Reactivation of Extensional E-W Faults with Cu Remobilisation
10 km